SCALE EFFECTS IN CAVITATING FLOW

Thesis by

Blaine Raphael Parkin

In Partial Fulfillment of the Requirements

For the Degree of

Doctor of Philosophy

California Institute of Technology

Pasadena, California

1952

ACKNOWLEDGEMENT

Many persons by their active interest and helpful criticism have aided the completion of this work. The writer wishes to thank Professor M. S. Plesset for his counsel throughout the course of this research.

The writer is indebted to many members of the research staff of the Hydrodynamics Laboratory for many helpful suggestions. He wishes to thank, in particular, Professor A. Hollander, Dr. Forrest Gilmore, and Mr. Haskell Shapiro for their valuable comments and criticisms. Mr. J. T. McGraw and Mr. R. W. Kermeen contributed greatly to the experimental program. Professor Stanley Frankel has given profitable advice in connection with the I. B. M. calculations.

The writer also wishes to acknowledge the aid of the Office of Naval Research in support of this study.

TABLE OF CONTENTS

ABSTRACT

Scale effects in cavitating flow are considered for the so-called limited cavitation flow regime. The roles of nuclei and air diffusion in ordinary water and the kinetic theory of liquids for pure water are considered as to their bearing on cavitation scale effects.

The attack on the problem is concentrated in three general areas. First, dynamic similarity considerations for individual bubble growth show that no useful scaling laws can be established from such arguments. Aside from changes due to Reynolds number, it is concluded that scale effects are dependent upon the time required for a nucleus to grow from its original microscopic size to a macroscopic size. Second, a series of experiments shows that the cavitation behaves in a systematic way as the scale of the immersed body is changed. In certain instances, the inception of cavitation depends on both model size and free stream velocity. Third, a theoretical study is made to gain insight into the relationships that must hold between the parameters which affect the inception of cavitation. A simplified theory gives only rough qualitative agreement with experiment.

PART I

INTRODUCTORY REMARKS

Introduction

Following Plesset[1]*, one can divide the flow of a liquid around a solid body into three regimes (Fig. 1). In the first regime, which is known as noncavitating flow, the liquid follows the classical hydrodynamic laws for an incompressible fluid. In the second regime, which may be called limited cavitation, the first manifestations of the coexistence of a gas or vapor phase with the liquid phase appear. In this case small discrete bubbles or areas occupied by foamy patches of gas or vapor first appear. The third regime, which is known as full cavity flow, is characterized by a single large vapor or gas cavity enveloping some portion of the body. In the following, the first appearance of limited cavitation will be called incipient cavitation. The study of the second, or limited cavitation, flow regime is the primary concern here.

The scaling laws which control the behavior of flows in the noncavitating regime have been well known for some time. For full cavity flows, Reichardt[2] has shown that the decisive quantity for determining the flow geometry is the cavitation number, $K = (p_o - p_v)/\frac{1}{2}\rho V_o^2$, where p_o and V_o are the free stream values of the static pressure and velocity respectively and ρ is the liquid density. Reichardt takes for p_v the sum of all gas pressures within the cavity. In the present work, p_v will denote only the liquid vapor pressure. However, for the limited cavitation

---

*Superscribed numbers in parentheses refer to the references listed in the bibliography.

flow regime, there is a definite lack of knowledge concerning the effects of body size, flow velocity, and dissolved air content upon the development of cavitation. In fact, it is now customary to employ the cavitation number, K, as the only significant parameter for describing all inviscid cavitating flows. It is shown in this paper by both theoretical and experimental means that the use of only the cavitation number for limited cavitation is an unjustified simplification.

The object of this study is to determine the behavior of limited cavitation on a given body shape placed in a rectilinear flow of constant free stream velocity. Such a flow is approximated in the test section of a water tunnel where the free stream velocity, free stream static pressure, and the amount of air dissolved in the water can be controlled as required. If one considers only this elementary flow configuration, very simple experiments can be performed. For such experiments, the spatial pressure distributions on the body surface will be known. From these known pressure distributions and the free stream velocity, pressure-time relationships can be calculated for a particle moving along the body surface with the liquid. From such pressure-time functions, one can study analytically the behavior of incipient cavitation with changing body scales.

Origin of Cavitation

For ordinary untreated water one assumes that there are nuclei containing air or water vapor, or both, which are stabilized on small, solid particles in the liquid. It is held that boiling or

cavitation must be initiated from such nuclei, since their absence would mean that very large surface tension forces must be overcome before cavitation can start. The slight tension under which cavitation normally occurs lends plausibility to arguments favoring the existence of the nuclei. If one supposes that cavitation originates from such small nuclei, then it must take them an appreciable time to grow to a macroscopic size. It is clear that this growth time must be dependent upon the pressure to which the nuclei are subjected. If for a constant free stream pressure and velocity only the scale of the immersed body is changed, the liquid flow may show corresponding changes in the cavitation due to changes in the time available for bubble growth.

On the other hand, one might suppose that if the water were saturated with air before entering the low pressure region of the body, there would be more time for air to diffuse into the cavitation bubbles, which move with the stream, as the scale of the body is enlarged. Presumably, this process could account for some changes in the nature of cavitation with scale. However, computations for air diffusion into bubbles have been made by P. S. Epstein and M. S. Plesset[3]. From their work it is found that for situations of practical interest the time required for the bubble to grow in any significant amount from pure diffusion is about one hundred times the period of existence of a cavitation bubble. If air diffusion can not significantly affect the growth of bubbles in ordinary cavitating flows, then one concludes again that cavitation scale effects, aside from Reynolds' number effects on the pressure distribution over the body, would result from

the non-zero growth time necessary for a nucleus to grow into a macroscopic bubble.

If it were possible to obtain a chemically pure liquid for cavitation experiments, the absence of air or vapor nuclei (in the sense outlined above) would dictate that one examine the kinetic theory of nucleation in considering all possible time-pressure effects for cavitating flows. However, in this instance the transition time from an initial steady nucleation rate to another such steady state, after an instantaneous change in pressure, has been shown by Zeldovich[4] to be of the order of 10^{-12} second. This result is supported by the recent work of Gilmore[5]. However, for the flow over a body, the time allowed for pressure changes is of the order of 10^{-3} second. The disparity in the time scales indicates that any variations in the state of the cavitation as a result of chemically pure water passing over geometrically similar models of different sizes cannot be influenced by nucleation effects. Further, for such pure substances, the liquid must actually be subjected to very large tensile stresses before it will cavitate, and these stresses are not even remotely approximated in cavitating flows of technical interest.

Under steady, or almost steady, conditions, ordinary untreated water has a definite boiling point and has no appreciable tensile strength. Such water will withstand tensions if it is subjected to transient low pressures of short duration. For water flowing around a solid body such short duration transient tensions can be produced on the water when it flows by the body surface. It is possible that the differences in the transient tensions produced by

changes in body length and free stream velocity can account for corresponding differences in the state of cavitation. It is the study of nucleus response under these transient pressure conditions that is of primary concern here.

PART II

SIMILARITY CONSIDERATIONS

Suppose that one visualizes two different spaces where typical units of distance, time, and mass are related by

$$r = k_1 \vec{r}_1$$

$$t = k_2 t_1 \tag{1}$$

$$m = k_3 m_1$$

The k's are constant factors which define the scale. Imagine that both spaces contain an inviscid incompressible liquid in which there are spherical bubbles of radius R = R(t) and $R_1 = R_1(t_1)$, respectively. The equation of motion[1] for such bubbles is given by

$$R\ddot{R} + \tfrac{3}{2}\dot{R}^2 = \tfrac{1}{\rho}\left[p(R) - P(t)\right] \tag{2}$$

where ρ is the liquid density, p(R) is the sum of all pressures at the bubble wall, and P(t) is the external pressure field in the liquid far from the bubble. The superscribed dots, as usual, stand for differentiations with respect to time. Let σ be the surface tension of water, p_v the vapor pressure corresponding to the temperature of the liquid, and p_a be the initial air pressure within the bubble before any growth from its initial size R_o has occurred. If the bubble is assumed to expand under isothermal conditions, then

$$p(R) = p_v - \frac{2\sigma}{R} + p_a\left(\frac{R_o}{R}\right)^3$$

Under the above assumptions, the bubble surface motion in each space is governed by

$$R\ddot{R} + \tfrac{3}{2}\dot{R}^2 = \frac{1}{\rho}\left[p_v + p_a\left(\frac{R_o}{R}\right)^3 - \frac{2\sigma}{R} - P(t)\right] \tag{3}$$

and

$$R_1\ddot{R}_1 + \tfrac{3}{2}R_1^2 = \frac{1}{\rho_1}\left[p_{v_1} + p_{a_1}\left(\frac{R_{o_1}}{R_1}\right) - \frac{2\sigma_1}{R_1} - P_1(t_1)\right] \tag{4}$$

These two motions, represented by (3) and (4), are said to be dynamically similar if one can proceed from Eq. (3) to Eq. (4), say, by multiplying each term of Eq. (3) by the same constant factor, a. This gives the equations

$$\text{(a)}\quad \frac{p_{v_1}}{\rho_1} = a\,\frac{p_v}{\rho} \qquad \text{(d)}\quad \frac{P_1(t_1)}{\rho_1} = a\,\frac{P(t)}{\rho}$$

$$\text{(b)}\quad \frac{p_{a_1}}{\rho_1}\left(\frac{R_{o_1}}{R_1}\right)^3 = a\,\frac{p_a}{\rho}\left(\frac{R_o}{R}\right)^3 \qquad \text{(e)}\quad \dot{R}_1^2 = a\dot{R}^2 \tag{5}$$

$$\text{(c)}\quad \frac{\sigma_1}{\rho_1 R_1} = a\,\frac{\sigma}{\rho R} \qquad \text{(f)}\quad R_1\ddot{R}_1 = aR\ddot{R}$$

To eliminate the constant, a, from these last equations (5) one can divide them all by (5e). This gives

$$\text{(a)} \quad \frac{p_{v_1}}{\rho_1 \dot{R}_1^2} = \frac{p_v}{\rho \dot{R}^2}$$

$$\text{(b)} \quad \frac{p_{a_1}}{\rho_1 \dot{R}_1^2}\left(\frac{R_{o_1}}{R_1}\right)^3 = \frac{p_a}{\rho \dot{R}^2}\left(\frac{R_o}{R}\right)^3$$

$$\text{(c)} \quad \frac{\sigma_1}{\rho_1 R_1 \dot{R}_1^2} = \frac{\sigma}{\rho R \dot{R}^2} \tag{6}$$

$$\text{(d)} \quad \frac{P_1(t_1)}{\rho_1 \dot{R}_1^2} = \frac{P(t)}{\rho \dot{R}^2}$$

$$\text{(e)} \quad \frac{R_1 \ddot{R}_1}{\dot{R}_1^2} = \frac{R \ddot{R}}{\dot{R}^2}$$

It is clear that (6e) is identically satisfied by (1). Also, by virtue of Eq. (1), (6b) is reduced to $p_{a_1}/\rho_1 R_1^2 = p_a/\rho R^2$. Combining this last expression with (6a) one gets

$$\frac{p_{v_1} + p_{a_1}}{\rho_1 \dot{R}^2} = \frac{p_v + p_a}{\rho \dot{R}^2} \tag{6f}$$

The addition of the ratios involving the air pressure and the vapor pressure serves only to group like terms. It is not intended that the four independent ratios shall be reduced in number. Although the combined ratios will be given a name, it must be remembered that even in the combined form, both parts must be matched separately. Equations (6f) and (6c) depend on properties of the liquid as well as

on the scale. Since P(t) is dependent upon the boundary conditions imposed upon the fluid, its behavior must be studied for the particular type of liquid flow that is imposed on the systems.

To summarize the results obtained thus far one can state that, if two bubbles are to grow in a dynamically similar manner, then both must have the same values of:

$$\frac{p_v + p_a}{\rho \dot{R}^2} = K_b \quad \text{, the bubble internal pressure number,}$$

$$\frac{\sigma}{\rho \dot{R}^2 R} = W_b \quad \text{, the bubble Weber number,}$$

and

$$\frac{P(t)}{\rho \dot{R}^2} = C_t \quad \text{, the bubble external pressure number. *}$$

This matching requirement is a very stringent condition which cannot be easily satisfied.

---

* There is no uniqueness in the definitions of the dimensionless ratios K_b, W_b and C_t. Further, it may be convenient to combine them. For example, $K_b/W_b = (p_v + p_a) \cdot R/\sigma$ must also be constant if the motions of the bubble wall are to be dynamically similar in any two cases. Similar conditions can be found from other ratios. The forms exhibited in the text were chosen because of their more familiar appearance. It can also be observed that if the quantity, $K_b - W_b - C_t$, is formed and solved for R, we have the result that the velocity is equal to the square root of the total pressure acting across the bubble wall, where the total pressure H, is given by $1/\rho \left[p_v + p_a - \sigma/R - P(t)\right]$. Further, if the motion is dynamically similar for two distinct cases, 1 and 2, then $\dot{R}_1/\dot{R}_2 = \sqrt{H_1/H_2}$, which from Eq. (1) becomes $\sqrt{H_1/H_2} = (k_1/k_2)$, a constant for the entire motion.

Suppose that in a steady inviscid rectilinear flow, cavitation is produced by putting a body in the stream. Cavitation bubbles will appear on those portions of the body where the pressure is close to the liquid vapor pressure. The time that a bubble spends in the region of low pressure is proportional to ℓ/V_o, where ℓ is a characteristic body length and V_o is the liquid velocity far upstream from the body. On the other hand, the magnitude of P(t) is proportional to V_o^2. It is, therefore, not possible to match C_t for two geometrically similar bodies of different size in flows of the same liquid even if K_b and W_b are matched. Accordingly, one may conclude that, for flows of the same liquid around geometrically similar bodies, dynamically similar growth of the individual bubbles cannot be expected to obtain.

It must be emphasized that, in the above discussion, the role of viscous effects has been neglected. To consider such effects one should also match the Reynolds numbers of the flow about the similar bodies and of the flow about the bubbles. For sufficiently fine bodies at small angles of attack, it is well known that the pressure coefficient, $C_p = (p - p_o)/\frac{1}{2}\rho V_o^{2*}$ is practically independent of the free stream velocity, V_o, over a wide range of Reynolds numbers. The viscous effects are important for individual bubbles only for very small radii[5] (e.g., $R = 10^{-4}$ cm). For bubbles of macroscopic size (e.g., R = 1 mm), the effects of viscosity can be neglected. Plesset and Gilmore[7] have found that if surface tension can be neglected, the macroscopic bubble size is not a sensitive function of its initial radius. Without any restrictions as to surface tension, B. E. Noltingk

---

*p is the pressure on the model surface and p_o is the free stream static pressure, while ρ is the liquid density as before.

and E. A. Neppiras[8] have found by trial from a series of electrical analog computations that, for a given initial radius, wide variations in the initial values of the bubble wall velocity, $\dot{R}$, produced insignificant changes in the bubble history. Viscous effects produce important changes only in the first part of the bubble growth, that is to say, the effective initial values are changed. Since the subsequent growth has been found to be practically independent of these initial values, it is possible to neglect altogether the effect of viscosity on bubbles growing in water.

It must be noted that in discussing the flow of bubble-containing water over a solid body, the tacit assumption that the bubble radius is much smaller than the body length has been made; that is, no pressure gradients are considered to be present in the vicinity of the water around the bubble. As a further idealization, any interaction between the pressure fields of the bubble and the body has been neglected (see, for example, Ref. 17, pp. 49-64). Further, experience shows that pressure gradients and the presence of the model cause large asymmetries in the shape of the larger bubbles (see Fig. 2). In fact, theoretical calculations by Rattray[9] have shown that the presence of a wall near a collapsing bubble is sufficient to cause large distortions in the bubble shape, even in the absence of pressure gradients. In addition, as the bubbles increase in size, the pressure gradients over the model give rise to a relative velocity between the bubble and the moving water, which further complicates the actual happenings. For the present, no account will be taken of these complications.

It was observed above, and it has also been pointed out by Gilmore and Plesset[7], that the time interval during which the bubble is exposed to a low-pressure region in which it can grow, is proportional to ℓ / V_o*. One must therefore expect the maximum size to which a bubble can grow to be directly dependent upon the scale, ℓ, if the velocity V_o is invariant. However, if both scale and velocity are changed, because the pressure decrease around the bubble varies as the square of the velocity, one cannot expect this simple scale dependence to hold.

It is now customary to regard the cavitation number

$$K = \frac{p_o - p_v}{\frac{1}{2}\rho V_o^2}$$

where p_o and V_o are the free stream values of static pressure and velocity, respectively, as the significant parameter for defining all cavitation modeling over geometrically similar shapes in the absence of viscous effects[10]. In those cases where it has been observed that discrepancies between prototype and model exist for the cavitation number at incipient cavitation, the discrepancies have been ascribed entirely to Reynolds number effects[11]. That such effects are important is undeniable. On the other hand, in view of the similarity arguments given above, there seems to be no reason for expecting the cavitation number to remain constant for incipient cavitation on similar shapes, even in the absence of viscosity.

---

*Gilmore and Plesset have also found that there may well be a dependence on scale of the number of cavitation bubbles formed on the body. However, it was not possible to test their findings by experiment, and no consideration will be given to this problem here.

PART III

EXPERIMENTAL INVESTIGATIONS

In order to look into the actual behavior of the effects of scale on cavitation, a series of experiments was initiated. To eliminate as many extraneous factors from the tests as possible, it was considered advisable to use a simple symmetrical two-dimensional airfoil shape which completely spans the 14-in. diameter working section of the Hydrodynamics Laboratory's High Speed Water Tunnel.[12] Blockage correction factors for the minimum pressure coefficients on the airfoils were computed using the work of Vincenti and Graham[13] and also of W. Perl and H. E. Moses[14] (see Appendix A). Later these theoretically predicted tunnel blockage factors were checked by experimentally obtained pressure distributions with fair agreement. Also, at this time, the independence for all practical purposes of the pressure distribution with Reynolds number for the attainable velocity range was checked.

The particular shape chosen for these tests was a 12°/o thick symmetrical Joukowski airfoil. This airfoil section was chosen because it was felt that for a given thickness it would cavitate more readily than some of the more modern, highly refined shapes, and thus allow for greater variation in the flow parameters p_o and V_o. Three airfoil models were made. They have chord lengths of 2, 4, and 8 inches. All models have a span of 14 inches. Pictures of these models are shown in Fig. 3, while the airfoil section and its theoretical pressure distribution will be found in Fig. 4.

In addition, the Hydrodynamics Laboratory already had some models of the NACA 4412 airfoil of 3-in. chord and 10-in. span,

which had been used by J. W. Daily[15] in other experiments. It was found possible to insert a lucite window in the upper working section side plate (see Fig. 5) and thereby obtain a profile view of the airfoils as cavitation bubbles developed on them. The initial high-speed motion pictures[16] were taken only of the upper or suction side of the hydrofoil using this setup. The sole purpose for using the NACA 4412 model was to observe the bubble asymmetries from the side. Successive runs were made at a V_o of 35, 40, and 50 fps and the angle of incidence was set at -4^o, 0^o, and $+4^o$ with the center line of the High Speed Water Tunnel working section. The -4^o angle corresponds closely to the zero lift angle for the NACA 4412. A typical photographic record and the resulting measured bubble growth is represented graphically in Fig. 6. There was no systematic dependence of bubble shape asymmetry on velocity and angle of attack, as can be seen from Table I. However, for one constant velocity, there was a dependence of average maximum bubble dimension on angle of attack (Table II). The results are not consistent enough and the data too meager to draw any conclusions as to the dependence of bubble size on velocity at constant angle of attack from these experiments.

Upon their completion, the Joukowski models were installed in the water tunnel working section to test for scale effects. High-speed motion pictures were taken of each model for at least two different values of the cavitation number K at a constant V_o of 40 fps. A schematic diagram showing the position of the camera relative to the model in the working section is shown in Fig. 7. As with the NACA 4412, the films were printed and measurements were made from the

prints. Such a graphical representation of the bubble growth for the 4-in. model is shown in Fig. 8. For each model the values of the maximum dimension transverse to the direction of the flow were averaged and these average values were plotted against model chord (Figs. 9 and 10). As can be seen from the graphs, at constant velocity the bubble size does increase with scale, as expected. Unfortunately the data are too sparse and the number of different scale sizes is too limited to make any detailed conclusions as to the precise nature of the variation. The data from the bubble histories are summarized in Table III.

In addition to the high-speed motion picture data, some observations were made by means of single flash still photographs. In this case, the shutter of the still camera was put on "bulb" and the very short duration single flash from the flash lamps was relied upon to expose the film. As can be seen from the pictures exhibited thus far, not all cavitation occurring on the hydrofoils is in the form of discrete bubbles. In fact, for the bodies used in these experiments, these large, well-defined bubbles are not nearly so common as the fine scale foamy cavitation which can be seen to coexist with the larger bubbles in the pictures (Fig. 2-a, for example). In regard to this fine scale cavitation, one can ask, if given two similar bodies of different sizes in a cavitating flow, will the relative portions of the bodies covered by this zone of cavitation be the same if both flows have the same cavitation number? To find the answer to this question all models were tested at a velocity

V_o, of 40 fps, and the free stream static pressure, p_o, was varied so that all degrees of cavitation were produced from no cavitation to the full cavity regime of flow. For each model the pressure range was divided into several strips and at each division point a picture and the pertinent flow data were taken. The length of the cavitation zone was measured and averaged from the pictures and expressed as a fraction of the chord length of the particular model. From the flow data the value of the cavitation parameter was computed and corrections for tunnel blockage* were applied. The resulting graph is given in Fig. 11. To serve as a check, five additional points were taken from random samples of the high-speed motion pictures of the Joukowsky airfoils. The graph of the results, though having considerable scatter, shows that the range of cavitation number K for each model is different. For example the eight-inch model shows cavitation for values of K in the range of the noncavitating flow regime for the two-inch model. In order that the cavitation number be the defining parameter for the geometric development of cavitation on the similar bodies, the first requirement is that the range of K be the same for all bodies. Fig. 11 shows that this is not the case and that at constant velocity the cavitation number for incipient cavitation changes with the scale of the body.

In order to check this change in the incipient cavitation number with changing scale, another set of experiments was made. Each model was tested at free stream velocities of 30, 40, 50, 60, 70, 80, and 90 fps, while the free stream pressure was varied until incipient

---

*See Appendix A.

cavitation had occurred. The pertinent flow parameters were then recorded. The values of the cavitation number for incipient cavitation were then computed and corrected for wall effect and plotted against Reynolds number based on the chord length (Fig. 12).

Data of a similar nature for axially symmetric flow around a series of bodies, which were formed by adding a hemispherical nose to a right circular cylinder of the same diameter as the nose, have been obtained by Kermeen and Stallkamp of the Hydrodynamics Laboratory*, California Institute of Technology. Models of various diameters were run at various velocities and the incipient cavitation point was found for each. The resulting cavitation numbers were plotted versus the Reynolds number, based on the model diameter for each model (Fig. 13).

There is much less scatter for these data than there is for the graph of the Joukowsky experiments. This is due to the fact that the point of incipient cavitation for these tests was obtained, not by visual observation, as was the case with the two-dimensional studies, but by measuring the sound intensity which results from cavitation in the liquid flow. A typical example of a curve of sound intensity versus cavitation number for the 2-in. diameter hemisphere-nosed model is shown in Fig. 14. The inception of cavitation corresponds to the peak sound level. As the cavitation number is lowered further and the cavitation over the model becomes more profuse, the intensity of the sound is seen to drop. It was found that for dissolved air concentrations near the saturation point at one atmosphere air pressure,

---

*A report of this study is being prepared by Mr. Kermeen and will be published in the near future.

the sound curves were reproducible. However, when the air concentration in the water was lowered to about half of the saturation value, a marked "hysteresis" effect was encountered. That is, if the cavitation was obtained by lowering the pressure p_o, it first occurred at a stage corresponding to a lower cavitation number than that for maximum noise intensity. Then, if the pressure was increased after the cavitation had been established, the sound would increase to its peak value. As the pressure was further increased, the cavitation would disappear. Here again, the curve was reproducible and Kermeen indicates that all incipient cavitation numbers were taken from curves in which the cavitation was first well established on the model and then the pressure was gradually raised until all cavitation had vanished. Fig. 13 was constructed using such sound curves.

It will be observed that the axially symmetric flow data very clearly show the change in incipient cavitation number with model size and flow velocity. The data from the Joukowski hydrofoils also show the variation of the incipient cavitation number with velocity but the dependence of the incipient cavitation number with model size is not conclusive. The reason for this failure is due to the fact that visual observation presents too great a chance for error for these two-dimensional shapes. There were apparent rough spots on the model which seemed to cause premature cavitation, and also the appearance of the cavitation changed from model to model and from velocity to velocity, so that one could never be sure that he was seeing corresponding cavitation states when the flow data were taken. We note then that these hydrofoil results partly contradict the results

found for the axially symmetric case and the results of Fig. 11, which motivated these last experiments. One may wish to disqualify comparison between the hemispherical headed bodies and the Joukowski hydrofoils on the ground that the effects on the pressure distribution due to viscosity are too pronounced for these axially symmetric shapes. However, a series of tests run in the water tunnel at the University of Iowa[17] showed only a 5°/o variation in the minimum C_p for a Reynolds number variation of from 1×10^5 to 6×10^5. From these Iowa tests the critical Reynolds number was found to be 2×10^5. One may thus conclude that, although there will be some Reynolds number effects for the data on the hemispheres, they should not mask essential trends of the cavitation results.

In the hope that the above mentioned conflicts could be resolved, the scaling experiments on the Joukowski hydrofoils were repeated, but instead of relying on visual observation as before, the sound measuring equipment (Appendix B) was employed in an attempt to find the point of incipient cavitation with greater consistency. However, it was found that the noise of vibration (Figs. 15 and 16) of the hydrofoils masked the lower frequency part of the cavitation noise spectrum and, of greater importance, the geometry of the flow was such that the hydrophone could not be focused in such a way that sound waves reflected from the working-section walls and the waves emanating from the opposite side of the model would be of negligible importance in the resulting intensity measurements. In other words, it was found that the peak noise intensity did not

necessarily correspond to the inception of cavitation. In addition, H. Shapiro, the designer of the sound-measuring equipment, has suggested that, for the measurements under question, there is a strong possibility that one or more of the amplifiers in the sound apparatus may have been overloaded. The only interesting results obtained from these experiments are presented in Fig. 17. This figure was obtained from the sound intensity versus cavitation number curves. A typical sound curve for the 2-in. chord Joukowski model is shown in Fig. 16. From the sound curves, ΔK, the change in cavitation number required to take the flow from incipient cavitation to the full cavity regime in each case, was plotted as a function of free stream velocity expressed in chord lengths per second. The ΔK values shown in the final figure contain an element of arbitrariness in their definition so that only the general trend exhibited in Fig. 17 is of significance. These results are another manifestation of the previously presented evidence that the bubble growth is affected by the scale of the cavitation-producing body.

The important results of the experiments may be summarized as follows. First, it was observed in connection with the high-speed motion picture studies that different cavitation numbers were required to obtain seemingly similar cavitation development on bodies of different size. This behavior was then confirmed at one free stream velocity for a range of cavitation numbers. Second, it was found that the inception of visible cavitation occurred for a very small change in the cavitation number K. That is, the transition from the non-cavitating flow regime to the regime of limited cavitation occurs

for a very small change in the cavitation number, as indicated by the sound curve, Fig. 14. Thus when the cavitation number is in a certain critical zone, very small changes in K completely alter the nature of the liquid flow. Third, a dependence of the inception of cavitation on free-stream velocity was found, and in certain instances, for constant velocity, a dependence of the incipient cavitation number on body scale was observed.

PART IV

THEORETICAL INVESTIGATIONS

The experimental results summarized above show that the cavitation number for incipient cavitation exhibits systematic changes with variations in the free-stream velocity, and that for some conditions the incipient cavitation number at constant free-stream velocity changes with the scale of the body. It is the purpose of this section to investigate the conditions for incipient cavitation by analytical means so that more precise ideas can be obtained about the relationships between the parameters which influence the behavior of the cavitation.

Basic Assumptions and Definitions

Before proceeding with the detailed formulation of the theory, a statement of the basic assumptions underlying the whole analysis is required.

First, viscous effects are entirely neglected in the present work. If experimental pressure distributions are available so that the minimum pressure on the body can be correlated with the Reynolds number, then one may take account of such variations in the minimum pressure coefficient in the calculations for incipient cavitation on any specific body using the procedures outlined below. It is known that the minimum pressures in the liquid occur on the immersed body. In fact the pressures decrease slightly as one proceeds through the boundary layer toward the body[18]. In view of the very small nucleus size it would seem that at least in the initial stages of bubble growth, the phenomena might be restricted entirely to the

boundary layer. Since definite knowledge is lacking on the effect of the boundary layer, it will not be considered here.

Second, the interaction between the flow around the expanding bubble and the flow of the liquid around the immersed body is not considered. Thus, the motion of the expanding bubble will be treated as though the liquid is infinite in all directions and the velocity and pressure relationships on the model will ignore the presence of cavitation. The effect of the flow around the body is related to the bubble growth through the P(t) term in the equation of motion for the bubble.

Third, the bubble is assumed to move with the fluid. For the very small bubbles considered here, buoyant forces are small and the viscous drag will be high so that any relative motion between the bubble and the water will be very small.

Fourth, the bubbles are assumed to be spherical.

In this study it is supposed that cavitation is initiated from small nuclei which contain air or water vapor, or both, stabilized on small solid particles in the liquid. In the noncavitating flow regime it is assumed that the nuclei do not have an opportunity to grow into bubbles of macroscopic or visible size. The difference, then, between the noncavitating and the cavitating flow regimes is that in the latter, the nuclei are exposed to a pressure environment favorable to bubble growth for a period sufficient to allow for the appearance of macroscopic bubbles. Consequently, one must consider two distinct problems in dealing with the matter of incipient cavitation. The first problem is the effect of free stream velocity, free stream static pressure, and body size in establishing a pressure environment favorable to bubble growth. The second problem is the response

(from Eq. (2)) of the nuclei to the transient low pressure created by the flow of water around the body. If the pressure distribution around the body is given, the first problem is trivial. In addition to difficulties of a purely mathematical nature, the second problem poses some questions about the physical properties of the nuclei for which no definite information is available.

Although it seems quite probable that the nuclei in a liquid have a range of sizes, it will be assumed here that all nuclei are of equal effective radius R_o. Incipient cavitation will be said to exist if a nucleus grows from its initial radius R_o to a radius of one millimeter during the time it is exposed to the low pressure which favors growth. This definition is arbitrary but it does have the virtue of being simple enough to work with. It is certainly not an absolute measure of a physical event, but this definition provides a framework within which the relationships between the relevant physical parameters which influence the inception of cavitation may be investigated. If one uses this definition, the problem of finding the conditions for incipient cavitation is: Given a fixed time for growth, determined by the free stream velocity and body size, what must be the free stream static pressure, p_o (and hence K), so that the required bubble growth will just take place?

Stability of Gas Nuclei

For practically all cases of technical interest, the water will contain dissolved air. Accordingly, the nuclei will contain air as well as water vapor. However, if surface tension forces act on these small bubbles, the air will be driven from the nuclei into solution with the surrounding water. That is to say, if the air or vapor bubbles are entirely surrounded by water, and if buoyancy is neglected, the gas will be

continually driven into solution until the bubbles vanish[2]. On the other hand, if the air is stabilized on small solid particles in the liquid the pressure due to surface tension must be zero or the three-phase nucleus could not exist as a stable thermodynamic structure. Therefore, if the surface tension pressure is initially zero, the nuclei can exist indefinitely, and by Henry's Law[20] the initial air pressure in the gas pocket is proportional to the concentration of air dissolved in the water. (See Fig. 18). As the bubble grows from its initial effective radius R_o, the pressure due to surface tension will increase until the full value, $2\sigma/R$, of the pressure due to surface tension is reached. Here σ is the coefficient of surface tension and R is the bubble radius, as before. The required behavior of the surface tension pressure may be approximated by $p_\sigma = 2S(R,\sigma)/R$ where the "surface tension law", $S(R,\sigma)$, is characterized by $S(R_o,\sigma) = 0$ and $S(R_1,\sigma) = \sigma$. R_1 is that bubble radius at which the surface tension law first achieves its full value. It is convenient to put $R_1 = nR_o$. The simplest assumption which will approximate the complex variation of the surface tension law with bubble growth, is that $S(R,\sigma)$ is a linear function of R. Then $S = (R-R_o)\sigma/R_o(n-1)$ for $R_o \leq R \leq n R_o$ and $S = \sigma$ when $R \geq n R_o$. If one puts $r = R/R_o$, then the surface tension law can be written in the form

$$S = \begin{cases} \frac{r-1}{n-1}\,\sigma & 1 \leq r \leq n \\ \sigma & r \geq n \end{cases}, \qquad (6)$$

It must be borne in mind that the surface tension law defined above is in a sense an attempt to account for an average behavior of a large number of nuclei of many possible initial sizes. Compared to

the atomic or molecular scale, the nuclei are macroscopic structures and hence the laws of surface tension for macroscopic systems are applicable. It has been argued that in order that such systems may exist in a stable state it is necessary to add a solid phase to the gas-water system and this has resulted in the introduction of another parameter, namely, the slope, 1/n, of the surface tension law. The reason for ascribing an average behavior to such a large number of nuclei with many possible initial sizes is because of the experimental fact that the zone of cavitation numbers at which cavitation starts is very narrow. That is, for a given flow configuration it is experimentally possible to assign a definite value of the cavitation number for the inception of cavitation.

Primary Parameters and Pressure-Time Relationships

The problem then is to study the behavior of the "average" nucleus in the transient pressure regions caused by the flow of the nuclei-containing water around submerged bodies of various sizes at various flow velocities. Thus, the relationships between a large number of parameters must be studied in order to obtain approximate quantitative results which may then be used to guide further experimental work. In particular, one must study the behavior of estimates for the initial size, R_o, with changes in the slope of the surface tension law (1/n). Next, the changes in the predicted values of the incipient cavitation number for changes in slope of the surface tension law must be estimated. Further, the sensitivity of the incipient cavitation number to changes in the initial air pressure in the nucleus and to changes in slope of the surface tension law must be at least qualitatively determined. Unfortunately, almost no reliable experimental data for

the effect of dissolved air content upon the inception of cavitation are now available.

No exact account can be taken of the many pressure distributions which can arise from all of the various body shapes which one may wish to consider in a liquid flow. However, the general falling and then rising of the pressure, common to all such bodies, will be approximated by two parabola-like curves joined at the point of minimum pressure. The term "parabola-like" is used because the actual functions used will be parabolic in time and the resulting spatial pressure distributions will differ slightly from the true parabolic shape. Two curves joined at the minimum pressure point are used so that actual pressure distributions, which are seldom symmetrical about the minimum pressure point, can be more closely matched.

Next, certain conditions will be obtained which will enable the "parabolic" pressure distribution to be replaced by a dynamically equivalent step function pressure distribution. The detailed numerical integrations of the equation of motion for the bubble will be made by using this further simplification. Two distinct advantages are gained by the use of the step function. First, it turns out that for a fixed n, or surface tension law slope, if the parabolic approximation is used, a three parameter family of solutions for Eq. (2) must be found. However, when the step function pressure distribution is used only a two parameter family of solutions is required. Second, the use of the equivalent step function allows one to find certain important relationships between the primary parameters

involved in the problem. This could not be done if the pressure distribution were not a constant in some time interval.

It was mentioned above that the only connection between the bubble growth and the liquid flow over the body is the choice of P(t) in the equation of motion for the bubble wall. For the step function pressure distribution it is evident that P(t) can be written as

$$P(t) = \begin{cases} p_o & t < 0 \quad , \\ p_o - \frac{1}{2}\rho V_o^2 a & t \geq 0 \quad , \end{cases} \tag{7}$$

where p_o and V_o are the free stream static pressure and velocity, respectively, and ρ is the liquid density. The quantity a is the magnitude of the pressure coefficient in the low pressure region. Fig. 19 shows the step function pressure law.

If it is remembered that the bubble is assumed to grow isothermally, and if account is taken of Eqs. (6) and (7), the equation of motion (Eq. (2) or Eq. (3)) becomes

$$R\ddot{R} + \frac{3}{2}\dot{R}^2 = \frac{1}{\rho}\left[p_v + p_a\left(\frac{R_o}{R}\right)^3 - 2\frac{S(R,\sigma)}{R} - p_o + \frac{1}{2}\rho V_o^2 a\right], \quad t>0 \ . \tag{8}$$

The initial conditions are $R(0) = R_o$ and $\dot{R}(0) = 0$. It may be noted that the initial air pressure in the nucleus, p_a, is given by Henry's Law, $p_a = \beta c$, where c is the concentration of air dissolved in the water and β is the Henry's Law constant.

Estimates for Initial Effective Bubble Radius

From inspection of Eq. (8) one sees that the forces tending to retard the bubble growth are a maximum at $R = nR_o$. If the bubble grows in such a manner that R just reaches nR_o with zero velocity,

it turns out that the time required for such growth will be infinite and cavitation will not occur. On the other hand, if the forces reach equilibrium when $R = nR_o$, the bubble growth will be little influenced by the retarding forces and cavitation will be well started. One can use this condition of force equilibrium together with experimental values for cavitating flow to obtain an estimate of the initial radius R_o. Thus, setting the right hand side of Eq. (8) equal to zero, one finds that for $R = nR_o$

$$p_v - p_o + \frac{1}{2}\rho V_o^2 a + \frac{p_a}{n^3} - \frac{2\sigma}{nR_o} = 0 \quad , \quad \text{or}$$

$$(a - K)\frac{1}{2}\rho V_o^2 + \frac{p_a}{n^3} - \frac{2\sigma}{nR_o} = 0 \quad ,$$

where K is the cavitation number, $(p_o - p_v)/1/2\rho V_o^2$. Experimental values of K and V_o were taken from the data for incipient cavitation number for the Joukowski hydrofoils, and curves of R_o versus n for various air contents, p_a, were calculated. The results are shown in Fig. 20. (V_o = 30 fps = 914 cm/sec, K = .30, σ = 70 dynes/cm, a = .53). Inspection of the R_o vs. n curves shows that except for the case of no dissolved air in the water, the variations in R_o with n are not large. Further since R_o is given by

$$R_o = \frac{2\sigma}{n(a-K)\frac{1}{2}\rho V^2 + \frac{p_a}{n^2}} \quad ,$$

an underestimate of the quantity (a - K) results in an overestimate of R_o. In using experimental values of (a - K) for incipient cavitation, one must recognize that such an underestimate of (a - K) is being made. The chief value of the calculations is that they show that an initial radius of the order of 10^{-4} cm is reasonable. They do not

relieve one of the task of arbitrarily choosing a value for R_o when he wishes to make numerical computations for bubble growth.

Critical Conditions for Cavitation

As was mentioned above, the forces tending to retard bubble growth reach a maximum at $R = nR_o$, with the result that for certain values of the coefficients in the equation of motion (8) cavitation will not occur. Before deriving relationships between the coefficients, the equation of motion will be rewritten in dimensionless form. Putting $r = R(t)/R_o$ and $\tau = t\sqrt{2\sigma/\rho R_o^3}$ Eq. (8) becomes

$$r\frac{d^2r}{d\tau^2} + \frac{3}{2}\left(\frac{dr}{d\tau}\right)^2 = \alpha + \frac{\gamma}{r^3} - \begin{cases} \dfrac{r-1}{(n-1)r} & , \ r \leq n \ , \\ \dfrac{1}{r} & , \ r \geq n \ , \end{cases} \tag{9}$$

where the "bubble driving parameter" α is given by

$$\alpha = \frac{p_v - p_o + \frac{1}{2}\rho V_o^2 a}{2\sigma/R_o} = (a-K)\frac{R_o \rho V_o^2}{4\sigma} \ , \tag{10}$$

and the "air content parameter" γ is

$$\gamma = \frac{p_a}{2\sigma/R_o} \ . \tag{11}$$

The initial conditions are then

$$r(0) = 1 \ , \qquad \frac{dr(0)}{d\tau} = 0 \ . \tag{12}$$

By recognizing that

$$r\frac{d^2r}{d\tau^2} + \frac{3}{2}\left(\frac{dr}{d\tau}\right)^2 = \frac{1}{2r^2}\frac{d}{dr}\left[r^3\left(\frac{dr}{d\tau}\right)\right] \ ,$$

one can write the first integral of Eq. (9) as

$$\frac{1}{2}r^3\left(\frac{dr}{d\tau}\right)^2 = \frac{\alpha}{3}(r^3-1) + \gamma \ln r - \begin{cases} \frac{1}{n-1}\left(\frac{r^3-1}{3} - \frac{r^2-1}{2}\right), & r \leq n \\ \frac{r^2}{2} - \frac{n^2+n+1}{6}, & r \geq n \end{cases} \quad (13)$$

where the initial conditions $dr(0)/d\tau = 0$ and $r(0) = 1$ have been used and the two integrals have been matched at $r = n$. Since (13) is a spatial integral of Eq. (9), Eq. (13) simply states that the change in the kinetic energy during the expansion is equal to the work done in the course of the motion. If one lets $W(r)$ represent the terms on the right hand side of Eq. (13), then for small enough values of the bubble driving parameter, α, the function $W(r)$ is very near a cubic polynomial, as shown schematically in Fig. 21. The value of r for which W has its isolated minimum will be called r_1. It can be shown that for n greater than 1 the minimum of W occurs at a value of r_1 greater than n. Since the kinetic energy is zero for $r = 1$, it will again be zero at the minimum of W if $W_{min} = 0$. It can also be shown that the time required for the bubble to grow to the value r_1, which corresponds to a zero minimum of W, is logarithmically infinite. Thus, if the bubble driving parameter, α, and the bubble air content parameter, γ, are chosen in such a way that $W_{min} = 0$, then cavitation will not occur under any circumstance. One may call such values of the bubble-driving parameter, α, and the bubble air content parameter, γ, critical values. These critical values are denoted by α_c and γ_c, respectively. A relationship between the critical values α_c and γ_c will now be found from the conditions $W(r_1) = 0$ and $dW(r_1)/dr = 0$.

From Eq. (13) the minimum conditions give

$$W(r_1) = \frac{\alpha_c}{3}(r_1^3 - 1) + \gamma_c \ln r_1 - \frac{r_1^2}{2} + \frac{n^2+n+1}{6} = 0$$

and

$$\frac{dW(r_1)}{dr} = \alpha_c r_1^2 + \frac{\gamma_c}{r_1} - r_1 = 0$$

Because the minimum occurs for $r_1 > n$, only the part of the integral (13) for $r \geqq n$ is required. If r_1 is regarded as a fixed parameter, α_c and γ_c are given in the parametric form,

$$\alpha_c = \frac{\frac{r_1^2}{2} - r_1^2 \ln r_1 - \frac{n^2+n+1}{6}}{\frac{r_1^3-1}{3} - r_1^3 \ln r_1} \quad , \tag{14}$$

and

$$\gamma_c = r_1^2 - \alpha_c r_1^3 \quad .$$

The minimum value of r_1 corresponds to $\gamma_c = 0$ and the root of $0 = r_1^2 - \alpha_c r_1^2$ of physical significance is $r_1 = 1/\alpha_c$. Substituting this result from the last of Eqs. (14) into the first of Eqs. (14) gives

$$\alpha_c^3 - \frac{n^2+n+1}{2}\alpha_c^2 + \frac{1}{2} = 0 \ , \quad \gamma_c = 0 \ . \tag{14a}$$

Equation (14a) has one real root for α_c. When α_c is real, it is expedient to solve for n in terms of α_c. Since $n \geqq 1$, Eq. (14a) gives for the positive root,

$$n = \frac{1}{2}\left[\frac{\sqrt{8\alpha_c^3 - 3\alpha_c^2 + 4}}{\alpha_c} - 1\right] \quad .$$

Taking values of α_c from 0.1 to 1.0, one finds the corresponding values of n and r_1. These results were plotted. For various fixed values of the surface tension slope number, n, the values of r_1 and α_c for $\gamma_c = 0$ were taken from this curve and then larger values of r_1 were selected to compute α_c and γ_c from Eqs. (14). The results of these computations are graphically presented in Fig. 22. These curves of the critical driving parameter, α_c, as a function of the critical air-content parameter, γ_c, are the loci of points for which the time required for a bubble to grow from its initial size to a size of nR_o (or larger) is infinite. For example, if for a given slope (1/n) of the surface tension law, a value of α greater than α_c is chosen at a fixed value of the air content parameter, γ, a finite time will be required for a bubble to reach a definite radius. However, if the slope of the surface tension curve is increased (n decreased) the bubble growth time will become greater and greater until the bubble-driving parameter, α, corresponds to the value α_c for some decreased value of n. In this case the time required for the growth will be infinite.

Numerical Calculations with the Step Function Pressure Law

In order that definite numerical calculations can be made, values of n and R_o must be chosen. If the original bubble is stabilized on only a portion of an unwetted solid particle, it seems plausible that the bubble must grow to several times its initial size before the surface tension law reaches its full value σ. For the present calculations a value of 5 will be taken for the parameter, n, in the surface tension law. If one takes account of the overestimate contained

in the curves of R_o versus n (Fig. 20), a value for the initial effective radius, R_o, of 2×10^4 cm. can be chosen.

In accordance with the definition of incipient cavitation given above, the bubble must grow to a macroscopic size of R = 1 millimeter. The total range of $r, (=R(t)/R_o)$ will then be from 1 to 500. The problem of determining the condition for incipient cavitation is now reduced to answering the following question. What time interval, as a function of the bubble-driving parameter α and the bubble air content parameter γ, is required for the bubble to reach a radius which is 500 times its initial value? To answer this question, one must find a two-parameter family of solutions of Eq. (13) of the form $\tau = F(\alpha, \gamma)$. The dimensionless time parameter, τ, is a function of the body length, free stream velocity and cavitation number. The air content parameter γ will be given, and α, the bubble-driving parameter, is a function of the cavitation number and free stream velocity. Then if $\tau = F(\alpha, \gamma)$ is known, a trial and error procedure will give the incipient cavitation number.

After such calculations for incipient cavitation number versus velocity have been made for different values of the air content parameter γ, comparisons between experimental results and the calculations could be used to obtain a measure of the success with which the surface tension law parameter, n, was chosen. It will be noticed from Fig. 22, that the slopes of the curves for critical bubble-driving parameter, α_c, versus the critical bubble air content parameter, γ_c, are steepest for low values of the surface tension law parameter. Thus, the initial air pressure in the nucleus will cause a greater change in

the cavitation number for incipient cavitation for steeper slopes of the surface tension law, $S(R,\sigma)$, than it will for a surface tension law with more gradual slope (large n). If sufficiently reliable data are available, a comparison with the calculated curves for incipient cavitation will suggest a better choice for the surface tension law parameter, n. Because there are almost no reliable data at this time, these alterations of the calculations will not be made here.

Equation (13) is easily reduced to quadratures, so that τ is given by

$$\tau = \int_1^5 \frac{r^{3/2}\,dr}{\sqrt{\frac{2}{3}\alpha(r^3-1) + 2\gamma \ln r - \frac{2}{n\,1}\left(\frac{r^3-1}{3} + \frac{r^2-1}{2}\right)}} + \int_5^{500} \frac{r^{3/2}\,dr}{\sqrt{\frac{2}{3}\alpha(r^3-1) + 2\gamma \ln r - 2\left(\frac{r^2}{2} - \frac{n^2+n+1}{6}\right)}} \quad . \tag{15}$$

The two integrals arise because of the change in the surface tension law at r = n = 5. Because the variations in τ for small changes in α and γ are required, approximate representations for Eq. (15) will be of limited value for those cases where α is near the critical bubble-driving parameter α_c. In any event, precise numerical integrations are required for the first integral in Eq. (15).

For the range of the air-content parameter γ from 0 to 1.8, with corresponding values of the bubble-driving parameter, α, from .145 to .230, ninety-eight integrations of Eq. (15) were carried out on an I.B.M. calculator. From these results the functional relationship, $\tau = F(\alpha, \gamma)$, represented by Eq. (15), was plotted as in Fig.

23. Tabulated data from which the figure was made are given in Table V.

Properties of the "Parabolic" Pressure Function

Before the above results can be used, the question of the relationship between the highly idealized step function pressure distribution, as used in the above calculations, and a pressure distribution determined by a body immersed in the liquid must be considered. Suppose that the magnitude of the minimum pressure coefficient on the body is b. Then in many cases it will be possible to approximate the actual pressure distribution by two functions which are parabolic in time. One function which decreases from $C_p = 0$ to $C_p = -b$ and another function which increases from $C_p = -b$ to $C_p = 0$ will be employed. Two functions are used because the pressure distributions around actual bodies are seldom symmetrical in the streamwise direction. Fig. 24 shows the parabolic pressure distribution. The required results for the "parabolic" pressure distribution will now be obtained.

Decreasing part, $0 \geq C_p \geq -b$:

The equation of a time parabola which decreases from $C_p = 0$ to $C_p = -b$ in a time interval T may be written as

$$C_p(t) = -b\left[2\frac{t}{T} - \left(\frac{t}{T}\right)^2\right] \tag{16}$$

where t is any time in the interval $0 \leq t \leq T$. (Fig. 24). From the Bernoulli equation $dx/dt = V = V_o\sqrt{1 - C_p(x)}$.* Under the conditions

---

*x is the distance along the stream line adjacent to the body.

$x = x(t)$, with $dx/dt \neq 0$ one may write $dx/dt = V_o \sqrt{1 - C_p(t)}$. If $x(0) = 0$ and $x(T) = \ell_1$, one obtains

$$\frac{\ell_1}{T V_o \sqrt{b}} = \int_0^1 \sqrt{\frac{1+b}{b} - \left(1 - \frac{t}{T}\right)^2} \; d\left(\frac{t}{T}\right)$$

or

$$T = \frac{2\ell_1}{V_o \left(\sqrt{\frac{1}{b}} + \frac{1+b}{b} \sin^{-1} \sqrt{\frac{b}{1+b}}\right) \sqrt{b}} \qquad (17)$$

When $C_p = -K$, that is, the pressure coefficient on the body is equal to minus the cavitation number for the flow, the pressure in the water around the bubble is equal to the vapor pressure of the water. Inspection of Eq. (8) shows that the bubble can not start to expand until the bubble has reached a point on the model where $C_p = -K$. The region for which $C_p \leq -K$ will be called the region of "favorable environment" for bubble growth. Thus the time that is of concern here is the time that the bubble is in a favorable environment. The value of (t/T) for which $C_p = -K$ is obtained directly from Eq. (16). If t_1 is the required value of the time, then

$$1 - \frac{t_1}{T} = \sqrt{\frac{b-K}{b}}$$

But the time interval Δt_1 spent by the bubble in the favorable environment is $(T - t_1)$. Hence $\Delta t_1 = T \sqrt{(b - K)/b}$, or substituting for T one finds

$$\Delta t_1 = \frac{2\ell_1 \sqrt{b-k}}{V_o \left[\sqrt{b} + (1+b) \sin^{-1} \sqrt{\frac{b}{1+b}}\right]} \qquad (18)$$

The relationship x = x(t) can be found by suitably altering the limits of integration in the integral leading to Eq. (17). If Eq. (17) is solved for ℓ_1 and divided into the result for x = x(t), there results

$$\frac{x}{\ell_1} = 1 - \frac{\left(1-\frac{t}{T}\right)\sqrt{\frac{1+b}{b}-\left(1-\frac{t}{T}\right)^2} + \frac{1+b}{b}\sin^{-1}\left(1-\frac{t}{T}\right)\sqrt{\frac{b}{1+b}}}{\sqrt{\frac{1}{b}} + \frac{1+b}{b}\sin^{-1}\sqrt{\frac{b}{1+b}}} \quad . \tag{19}$$

Increasing part, $-b \leq C_p \leq 0$:

For the portion of the pressure distribution downstream from the minimum pressure point one can write

$$C_p(t) = \frac{b}{(m-1)^2}\left[\left(\frac{t}{T}-1\right)^2 - (m-1)^2\right] \quad , \tag{20}$$

where $1 \leq \frac{t}{T} \leq m$. Thus $C_p(T) = -b$ and $C_p(mT) = 0$. In a manner similar to that used in obtaining Eq. (17), the analogous result

$$(m-1)T = \frac{2\ell_2}{V_o\left(\sqrt{\frac{1}{b}} + \frac{1+b}{b}\sin^{-1}\sqrt{\frac{b}{1+b}}\right)\sqrt{b}} \tag{21}$$

is obtained. Here ℓ_2 is the distance along the stream line next to the body from the point where $C_p = -b$ to the point where again $C_p = 0$, and T is given by Eq. (17). The time t_2 at which $C_p = -K$ is obtained from Eq. (20);

$$\frac{t_2}{T} - 1 = (m-1)\sqrt{\frac{b-K}{b}}$$

Thus the period spent by the bubble in the favorable environment for this portion of the pressure distribution is given by $\Delta t_2 = (t_2 - T)$. Substitution for (m - 1)T from Eq. (21) yields

$$\Delta t_2 = \frac{2\,\ell_2\sqrt{b-K}}{V_o\left[b + (1+b)\sin^{-1}\sqrt{\frac{b}{1+b}}\right]} \quad . \tag{22}$$

As before, the space-time relationship can be found in a manner similar to that employed in deriving Eq. (19). Thus,

$$\frac{x}{\ell_2} = \frac{\theta\sqrt{\frac{1+b}{b} - \theta^2} + \frac{1+b}{b}\sin^{-1}\theta\sqrt{\frac{b}{1+b}}}{\sqrt{\frac{1}{b}} + \frac{1+b}{b}\sin^{-1}\sqrt{\frac{b}{1+b}}}, \qquad \theta = \frac{\frac{t}{T} - 1}{m-1} \quad , \tag{23}$$

where x is measured along the stream line from the point for which $C_p = -b$. From Eq. (17) the expression for T can be put into Eq. (21) to find m. This substitution gives

$$(m-1) = \frac{\ell_2}{\ell_1} \quad . \tag{24}$$

The "parabolic" curves are compared with the Joukowski and the "Hemisphere" experimental pressure distributions in Figs. 26 and 28. Equations (18) and (22) can be added to find the total time, $\Delta t = \Delta t_1 + \Delta t_2$, that a bubble spends in the whole region of favorable environment, and one finds

$$\Delta t = \frac{2(\ell_1 + \ell_2)\sqrt{b-K}}{V_o\left(\sqrt{b} + (1+b)\sin^{-1}\sqrt{\frac{b}{1+b}}\right)} \quad . \tag{25}$$

It is this value of the time Δt which determines the dimensionless time τ. For a given pressure distribution, ℓ_1, ℓ_2, and b are known quantities and V_o, the free stream velocity, will be given so that K is the only unknown factor required to find Δt or τ.

Dynamic Equivalence between the Step and "Parabolic" Pressure Laws

The preceding preliminary calculations now make it possible to approximate the relationship which must obtain between the idealized step function pressure distribution and the more realistic "parabola-like" pressure distribution if the essential features of the bubble growths are to be the same in both cases. The matching will consist of two parts. First, the time spent by the bubble in the low pressure region will be taken to be the same for both the step function and the parabolic pressure laws. Second, the equation of motion (2) will be integrated in closed form by approximate means for both the step function and the parabolic pressure laws. The two approximate bubble histories will be said to be dynamically equivalent when the total bubble growths under the two pressure laws are equal. These two conditions will result in approximations of the required relationships between the step and parabolic pressure functions.

The first point of comparison for the two pressure laws is the relationship between the time intervals during which the nucleus is exposed to the favorable environment in each case. It will be specified that the time spent by the bubble in the favorable environment shall be the same for both the step function pressure law and the "parabolic" pressure distribution. In both instances the free stream velocity, V_o, will be identical. From Eq. (7), the pressure coefficient for the pressure step is

$$C_p = \begin{cases} 0 & \text{for } t < 0, \quad \text{or } x < 0, \\ -a & \text{for } t \geq 0, \quad \text{or } x \geq 0. \end{cases} \tag{26}$$

If the bubble is assumed to grow in an interval $0 \leq x \leq \lambda$ then the same

reasoning which gave Eq. (17) gives $\Delta t = \frac{\lambda}{V_o \sqrt{1+a}}$. Equating this result to the Δt of Eq. (25) gives

$$\frac{\lambda}{\sqrt{1+a}} = \frac{2(\ell_1 + \ell_2)\sqrt{b-K}}{\sqrt{b} + (1+b)\sin^{-1}\sqrt{\frac{b}{1+b}}} \tag{27}$$

If a relationship between a and b can be found, then λ will be given in terms of known quantities.

The second point of comparison is the requirement that the total bubble growth in the time interval of favorable environment must be the same for the two pressure functions. This requirement, which will result in a relationship between a and b, will be called dynamical equivalence. The a priori derivation of an exact condition for the dynamical equivalence of the two cases is formidable in view of the fact that to obtain such a precise result the equation of motion (3) must be integrated in exact analytical form. It will be worthwhile to use an approximate method of integration due to M. S. Plesset[19]. Plesset's method, while lacking rigorous justification, has been shown to give results in close agreement with precise numerical results if the right-hand side of the dynamical Eq. (3) is a function which increases exponentially with time. The approximation is based on the supposition that the right-hand side of the equation of motion, Eq. (2), is a monotonic function of time and it is felt that when this condition is met, the agreement between the exact numerical results and the approximate solution will be close. It is unfortunate that this condition will not be entirely satisfied here. After

obtaining the required approximate result, it will be used to define a pair of dynamically equivalent pressure distributions so that numerical integrations can be performed to test the reasonableness of the approximate method.

The equations of motion applied to each case differ only in the form of the forcing function on the right-hand side, because in one case a step function is taken while in the other case a "parabolic" dependence is assumed. Thus it seems reasonable that in comparing the behavior in the two cases, one can discard the surface tension and air content terms. This approximation may be partially justified by recognition of the fact that both the surface tension and the air content terms decrease very rapidly as the bubble grows. Thus Eq. (3) can be written in the form

$$R\ddot{R} + \frac{3}{2}\dot{R}^2 = g(t) \tag{28}$$

where g(t) is given for the step function case by

$$g(t) = \begin{cases} \frac{1}{2}V_o^2(-K) , & t<0 , \\ \frac{1}{2}V_o^2(a-K) , & t\geq 0 , \end{cases} \tag{29}$$

and for the parabolic case by

$$g(t) = \tfrac{1}{2}V_o^2 b\left[\frac{b-K}{b} - \left(1-\frac{t}{T}\right)^2\right] , \tag{30}$$

with $$0 \leq \left(1-\frac{t}{T}\right) \leq \sqrt{\frac{b-K}{b}} .$$

Equation (30) accounts for only the portion of the parabolic pressure curve lying upstream from the minimum pressure point which is in the region of favorable environment. The growth in the

second portion of the parabolic pressure curve will be accounted for by approximating the slope of the growth curve at the minimum pressure point and multiplying this slope by the time interval of favorable environment Δt_2 (Eq. 22).

Plesset's approximate integration method is based upon the assumption that in Eq. (28) g(t) is a function such that the acceleration of the bubble wall R does not become negative; then

$$R\ddot{R} = g(t) - \tfrac{3}{2}\dot{R}^2 \geq 0 \quad . \tag{31}$$

Consequently,

$$\dot{R}^2 \leq \tfrac{2}{3}\, g(t) \quad , \quad \text{or}$$

$$\dot{R} \leq \sqrt{\tfrac{2}{3}\, g(t)} \quad . \tag{32}$$

Integration of (32) gives

$$R - R_o \leq \int_{t_o}^{t} \sqrt{\tfrac{2}{3}\, g(\xi)}\; d\xi \quad , \tag{33}$$

where R_o is the radius at the initial time t_o. Now define a function $\phi(t)$ such that

$$R - R_o = \phi(t) \int_{t_o}^{t} \sqrt{\tfrac{2}{3}\, g(\xi)}\; d\xi = \phi(t)\, I(t) \tag{34}$$

Because of Eq. (33), the function $\phi(t)$ is of bounded variation:

$$0 \leq \phi(t) \leq 1 \quad . \tag{35}$$

Equation (34) is a formal solution to Eq. (28). Accordingly, substitution of (34) into Eq. (28) gives the exact differential equation,

$$(R_o + \phi I)(\ddot{\phi} I + 2\dot{\phi}\dot{I} + \phi \ddot{I}) + \tfrac{3}{2}(\dot{\phi} I + \phi \dot{I}) = \tfrac{3}{2}\dot{I}^2 \quad . \tag{36}$$

Equation (36) will now be approximated with the assumptions that

$$\ddot{\phi} I + 2\dot{\phi} I \ll \phi \dot{I} \quad ,$$

$$\dot{\phi} I \ll \phi \dot{I} \quad ,$$

and $$R_o \ll \phi I \quad .$$

A first approximation for ϕ is then given algebraically by Eq. (36). Solving for ϕ yields,

$$\phi \approx \frac{1}{\sqrt{1 + \frac{2I\dot{I}}{3\dot{I}^2}}} \quad . \tag{37}$$

This result, together with Eq. (34) gives the required approximate integration. In order that the parabolic case can be treated by means of the linear extension outlined above, the derivative dR(t)/dt must be found. Taking account of the inequalities preceding Eq. (37) the derivative is given by $\dot{R} \approx \phi \dot{I}$. From the results following Eq. (21) $\Delta t_2 = (t_2 - T) = (m - 1)\, T \sqrt{(b - K)/b}$ so that the linear growth to be added is

$$R(T)\,\Delta t_2 \approx \phi \dot{I}(T)(m-1)\,T\sqrt{\frac{b-K}{b}} \quad .$$

Hence the total growth in the parabolic case is

$$R - R_o = \phi(T)\left[I(T) + \dot{I}(T)(m-1)\,T\sqrt{\frac{b-K}{b}}\right] \quad . \tag{38}$$

Substituting the equation for g(t) (Eq. 30) into the integral for I(t),

$$I(t) = \int_{1-\sqrt{\frac{b}{b-K}}}^{\frac{t}{T}} \sqrt{\tfrac{2}{3}\cdot\tfrac{1}{2} V_o^2 b\left[\frac{b-K}{b} - (1-u)^2\right]}\; du$$

or putting

$$y = (1-u)\sqrt{\frac{b}{b-K}}$$

$$I(t) = -TV_o\sqrt{\frac{(b-k)^2}{3b}}\int_1^{(1-\frac{t}{T})\sqrt{\frac{b}{b-k}}}\sqrt{1-y^2}\;dy$$

$$= \frac{TV_o}{2}\sqrt{\frac{(b-k)^2}{3b}}\left[\left(1-\frac{t}{T}\right)\sqrt{\frac{b}{b-k}}\sqrt{1-\frac{b}{b-k}\left(1-\frac{t}{T}\right)^2}-\frac{\pi}{2}+\sin^{-1}\left(1-\frac{t}{T}\right)\sqrt{\frac{b}{b-k}}\right].$$

Hence,

$$I(T) = \frac{\pi}{4}TV_o\sqrt{\frac{(b-k)^2}{3b}} \quad . \tag{39}$$

From

$$\dot{I}(t) = V_o\sqrt{\frac{b-k}{3}}\sqrt{1-\frac{b}{b-k}\left(1-\frac{t}{T}\right)^2} \quad \text{and} \quad \ddot{I}(t) = -\frac{V_o\left(1-\frac{t}{T}\right)\sqrt{\frac{b-k}{3}}}{T\sqrt{1-\frac{b}{b-k}\left(1-\frac{t}{T}\right)^2}}$$

it follows that,

$$\dot{I}(T) = V_o\sqrt{\frac{b-k}{3}} \quad \text{and} \quad I(T) = 0 \quad . \tag{40}$$

From Eq. (40) and Eq. (37), $\phi(T) \approx 1$ so that $R - R_o$, Eq. (38), becomes

$$R - R_o \approx TV_o\left(\frac{\pi}{4}+m-1\right)\sqrt{\frac{(b-k)^2}{3b}} \tag{41}$$

for the parabolic case.

For the step function case g(t) is given by Eq. (39) so that

$$I(t) = \int_o^t \sqrt{\frac{2}{3}\;\frac{1}{2}V_o^2(a-k)}\;dt' \quad . \tag{42}$$

Because the time spent in the favorable environment is the same in this case as it is in the parabolic case, the time interval for Eq. (42) is equal to the Δt of Eq. (25). It is easy to see that $\Delta t = mT\sqrt{(b-K)/b}$ so that

$$I(\Delta t) = mV_o T \sqrt{\frac{(a-K)(b-K)}{3b}} \quad . \tag{43}$$

Inspection of Eq. (42) shows that $I(t) = 0$ so that $\phi(t) = 1$. For this case Eq. (34) alone suffices to give the approximate integration required, and hence

$$R - R_o = mV_o T \sqrt{\frac{(a-K)(b-K)}{3b}} \quad . \tag{44}$$

The requirement for dynamical equivalence can be applied to Eqs. (41) and (44) to give

$$m\sqrt{a-K} \approx \left(\frac{\pi}{4} + m - 1\right)\sqrt{b-K} \quad . \tag{45}$$

Thus, the relative shapes of the step and the parabolic pressure distributions are now specified by

$$\frac{\lambda}{\sqrt{1+a}} = \frac{2(\ell_1 + \ell_2)\sqrt{b-K}}{\sqrt{b} + (1+b)\sin^{-1}\sqrt{\frac{b}{1+b}}} \tag{27}$$

$$\sqrt{a-K} \approx \left(\frac{\frac{\pi}{4} + m - 1}{m}\right)\sqrt{b-K}$$

$$(m-1) = \frac{\ell_2}{\ell_1} \tag{45}$$

and (24)

The above matching conditions were checked for one case of incipient cavitation on the 2 inch Joukowski hydrofoil. From the trial and error calculations presented below (p. 49), it was found that when the free stream velocity is 16 meters per second the incipient cavitation number, K, is .403, and hence the bubble driving parameter, α, is .190 and the dimensionless time τ is 1400. The equation of motion (2) was integrated for the case where the air content parameter, γ, is 1.0, and the P(t) term is composed of the parabolic laws (16) and (20). The numerical solution gives a bubble diameter of 2/3 mm. at the end of the specified time interval. If the matching had been exact the final bubble diameter would have been 2 mm. The discrepancy arises since the condition $\ddot{R} \geqq 0$ is violated because of oscillations in the initial stages of bubble growth. The present approximate integrations start from the point where the external pressure equals the liquid vapor pressure. It is probable that a better approximation would have been obtained if the integrations used to approximate the growth under the parabolic pressure law had started from that radius and time at which the surface tension is first constant, and the external pressure is less than the vapor pressure by an amount equal to the surface tension pressure. Except for a constant factor the essential variations between the step function and parabolic pressure laws have been approximated in the above procedure and the approximate results will be used.

Scaling Laws for Incipient Cavitation at High Free Stream Velocity ($V_o \to \infty$)

It is now possible to obtain a relationship for cavitation scale effect for very large values of the velocity, V_o. As the free stream

velocity V_o becomes very large, the bubble-driving parameter, a, (see Eq. (10)) increases as V_o^2. From Eq. (25) it is clear that the time Δt (and hence τ since $\tau = \Delta t \sqrt{2\sigma/\rho R_o^3}$) decreases as $1/V_o$. Hence for $a >> 1$, Eq. (15) can be approximated by

$$\tau \approx \sqrt{\frac{3}{2\alpha}} \int_1^{500} dr \tag{46}$$

where $$\alpha = (a-K)\frac{R_o \rho V_o^2}{4\sigma} = \left(\frac{\pi}{4} + m - 1\right)\frac{R_o \rho V_o}{4\sigma}(b-K) \quad .$$

This result for a follows from Eqs. (10) and (45). From Eq. (25) the relation

$$\tau = \frac{2(\ell_1+\ell_2)\sqrt{b-K}}{V_o\left(\sqrt{b} + (1+b)\sin^{-1}\sqrt{\frac{b}{1+b}}\right)}\sqrt{\frac{2\sigma}{\rho R_o^3}} \quad , \quad \text{will be used for } \tau \text{ in Eq. (46).}$$

For geometrically similar bodies $(\ell_1 + \ell_2)$ will be some constant multiplied by the characteristic body length L. Using this fact and substituting for τ and a into Eq. (46) there results

$$\frac{L\sqrt{b-K}}{V_o} \approx \frac{C}{\sqrt{(b-K)V_o^2}} \tag{47}$$

where C is a constant. Suppose now that a given body running at very high velocity has a characteristic length L_o and is found to have an incipient cavitation number K_o. Then if another similar body in high speed flow has length L and incipient cavitation number, K, the relationship $(b-K_o)/(b-K) = L/L_o$ must hold. This last result can be written in the form

$$\frac{K}{K_o} = \frac{L_o}{L} + \frac{b}{K_o}\left(1 - \frac{L_o}{L}\right) \quad , \tag{48}$$

subject to the condition that V_o, the free stream velocity, is very high. Just how high the velocity V_o must be is determined from more detailed calculations below. A plot of K/K_o versus L/L_o is given in Fig. 25, for values of b/K_o from 1.0 to 2.0.

Calculations for Incipient Cavitation on the Joukowski Hydrofoils

Calculations for incipient cavitation on the Joukowski hydrofoils will now be made by means of the procedures developed above. The relationships which must be used for the numerical work are

$$\alpha = \left(\frac{\frac{\pi}{4} + m - 1}{m}\right)^2 \frac{R_o \rho V_o^2}{4\sigma}(b-K) \quad ;$$

$$(m-1) = \frac{\ell_2}{\ell_1} \quad ;$$

$$\tau = \frac{2(\ell_1 + \ell_2)\sqrt{b-K}}{V_o\left(\sqrt{b} + (1+b)\sin^{-1}\sqrt{\frac{b}{1+b}}\right)} \sqrt{\frac{2\sigma}{\rho R^3}} \quad ;$$

and a graph of the function $\tau = F(\alpha, \gamma)$, Fig. 23. In order to find m, the experimental pressure distributions for the three Joukowsky hydrofoils were corrected for tunnel blockage and a single curve was faired through the points as shown in Fig. 26. It was observed experimentally that the first visible cavitation on the hydrofoils occurred at about 20% of the chord, c, from the point where the pressure distribution C_p is first zero. In an effort to account for this experimental fact, the distance ℓ_2 was taken to be equal to .25c - ℓ_1. The length ℓ_1 was determined by measuring the distance from the minimum pressure point to that point where the pressure coefficient, C_p, is zero nearest to the leading edge of the hydrofoil. These measurements gave $\ell_2/\ell_1 = 14/11$ so that (m - 1) = 1.27. These geometric relationships and the approximating parabolic pressure distribution are shown in Fig. 26.

If one takes σ = 70 dynes/cm, $R_o = 2 \times 10^{-4}$ cm, ρ = 1 gram/cm^3, b = .53, the equation for the dimensionless time is

$$= 1.28 \times 10^6 \frac{c}{V_o} \sqrt{.53 - K} \quad ,$$

and for the bubble-driving parameter,

$$a = .581 \times 10^{-6} (.53 - K) V_o^2 \, .$$

By means of the graph for $\tau = F(a, \gamma)$, with γ = 1.0*, trial and error calculations were made to find K for values of the free stream velocity V_o of from 900 cm/sec to 3000 cm/sec for each of the three chord lengths, 2 inches (5.08 cm) 4 inches and 8 inches. The calculations were extended to infinite velocity by means of Eq. (47) (for this case C = 550 cm.). For the case c = 4 inches, the calculations were repeated for zero air content (γ = 0). From these calculations, curves of incipient cavitation number K versus the ratio c/V_o are given in Fig. 27. The calculated results are also compared with experiment in Fig. 27. The experimental scatter is too great to draw any definite conclusions as to the applicability of the theoretical results. The calculated curves show the tendency for the cavitation number to increase with velocity for all scales, and, except for the higher velocities, no scale effects are found at constant velocity. The data do not conclusively prove or disprove these theoretical findings.

Calculations for Incipient Cavitation on the "Hemispheres".

Calculations were made for the inception of cavitation on right-cylindrical bodies with hemispherical noses. The same body sizes

---

*γ = 1 corresponds to an initial bubble air pressure of 700 millibars or a dissolved air concentration of 70^o/o, the saturation concentration for an air pressure of 1 atmosphere above the water.

were selected as were used by R. W. Kermeen in his experiments (see Fig. 13). Kermeen found that the dissolved air concentration in the water during his experiments was about one half of the saturation value for an air pressure of one atmosphere. The corresponding value of the air content parameter, γ, was taken to be 0.7.

The experiments of Rouse[17] show that b, the absolute value of the minimum pressure coefficient on the body, increases from about .65 at a Reynolds number of $.6 \times 10^5$ to .74 when the Reynolds number is greater than or equal to 1.2×10^5. This change in the minimum pressure coefficient, b, was accounted for in the determinations of the dimensionless time, τ, (Eq. 25) and of the bubble-driving parameter, α, (Eqs. 10 and 45). The "parabolic" pressure distribution was fitted to the experimental pressure distribution by selecting for the pressure distribution asymmetry factor, m, a value of 1.45. Fig. 28 compares the experimental and the "parabolic" pressure distributions when the Reynolds number is in the supercritical regime ($R_e \geq 1.2 \times 10^5$). Trial and error calculations were then performed in the same fashion as for the Joukowski hydrofoils. The calculations are compared with Kermeen's data in Fig. 29. It will be seen that the calculated values of incipient cavitation number are in poor agreement with experiment. The disparity between the experimental and the calculated results increases as the size of the body decreases. There are two possible reasons for the disagreement. Either the mathematical approximations used in developing the theory are too great, or some physically important effect (such as that due to the boundary layer) has been overlooked. It may well be that both

of these factors contribute to the large differences between theory and experiment.

It will be noticed in Fig. 29 that for the 2, 1-1/8 and 1/4 inch models the experimental data for incipient cavitation number seem to show little or no dependence upon the free stream velocity, V_o, when V_o is greater than or equal to 80 feet per second. This apparent independence of the incipient cavitation number with free stream velocity corresponds to the theoretical conditions leading to Eq. (48). Eq. (48) relates the incipient cavitation number to the characteristic body length of similar bodies under the condition that the free stream velocity is very high. The incipient cavitation number under this condition is said to have attained its limiting value. If it is supposed that the experimental data, for the highest free stream velocities measured, approximate such limiting values of the incipient cavitation number it is reasonable to compare the experimental points for this case with Eq. (48). The data for incipient cavitation number on each model at the highest test velocity were averaged and plotted against model diameter in Fig. 30. Eq. (48) was then fitted to the experimental points twice, at diameters of 1/4 inch and of 2 inches respectively. The two curves are shown in Fig. 30. It will be seen that the agreement between experiment and theory is best when the calculations are fitted to the smallest model. The free stream velocity in all cases was at least 80 feet per second. Perhaps data for even higher values of V_o would give better agreement when the theory is compared with experiment. More experiments must be made to test this point. The theoretical

trends (Figs. 27 and 29) seem to indicate that the limiting value for the incipient cavitation number will be attained for higher velocities, V_o, for large bodies than for small models. If this trend is correct it means that most water tunnels cannot reach high enough speeds to make use of this theoretical approximation when models with low pressure regions larger than that of the two-inch diameter hemisphere are tested.

It will be recalled that in deriving Eq. (48), as with all other theoretical results, two basic approximations were made. First, the pressure was estimated from experimental results and Bernoulli's Law. Second, the time during which the nucleus is exposed to a low pressure condition where bubble growth can occur was estimated from the body length and the liquid velocity along the body just outside the boundary layer. The application of Bernoulli's Law should give quite accurate results. One must conclude therefore, that the time estimates are not good enough for the present purposes. Furthermore, if one traces through the calculation procedure for the inception of cavitation, he will find that underestimating the time results in an underestimate of the cavitation number for incipient cavitation. The present calculations do not account for the possibility that at least a portion of the bubble growth occurs in the boundary layer where the time available for growth would be greater than the time estimates used here. Thus, before one can make predictions for the inception of cavitation with confidence, the boundary layer's effect on growing cavitation bubbles must be understood.

PART V

CONCLUSIONS

It is found by experiment that cavitation on submerged bodies in a rectilinear flow shows decided changes in its development as the free stream velocity and body size are changed. For a given flow configuration, it is found that the inception of visible cavitation is obtained at essentially one cavitation number, K. That is, when the cavitation number is in a certain critical zone, very small changes in K completely alter the nature of the liquid flow from noncavitating to cavitating flow. It is found that under certain conditions the incipient cavitation number depends on both body scale and free stream velocity.

Similarity arguments show that one cannot obtain useful scaling laws for limited cavitation from such considerations. In fact, the similarity calculations show that one may expect limited cavitation to be affected by both body size and free stream velocity. One is then led to conclude that the cavitation number, K, is not the only significant parameter required to define the limited cavitation flow regime. Both experiment and analysis indicate that one must specify the model size, free stream velocity, dissolved air content and the cavitation number if he wishes to describe completely an experimental situation for an immersed body of specified shape. The condition of the body surface should also be specified, but this effect has not been considered in this paper. Although it is convenient to use the cavitation number, K, for theoretical calculations, one would be closer to the physical relationships if, instead of the cavitation parameter,

he specified the liquid vapor pressure and the free stream static pressure.

From the greatly simplified theoretical investigation presented in Part IV, one can conclude that the neglect of the role of the boundary layer is not justified for precise evaluation of the effects of model scale and free stream velocity upon the inception of cavitation. On the other hand, the qualitative agreement between the experimental and calculated trends for incipient cavitation number versus free stream velocity and body size, substantiates the basic premise that scale effects in limited cavitation arise because of transient pressure effects on the nuclei in the liquid flow.

A combination of simple theoretical considerations and some of the experimental data for incipient cavitation gives estimates for the effective initial nucleus radius. It is found that for the water used in the experiments, the calculated effective initial radius is between 10^{-4} and 10^{-3} centimeter.

For the limiting case where the free stream velocity approaches infinity, it is found that the cavitation number, K, for incipient cavitation does not approach b, the absolute value of the minimum pressure coefficient on the submerged body. Instead, the limiting value of the incipient cavitation number approaches a value less than b, and the difference b - K is found to be inversely proportional to the characteristic body length, L. The theory closely approximates the experimental results if the equation is fitted to the data for the smallest model. More experimental work is needed to demonstrate the complete validity of this result.

It is useful to note that the usual design procedure by which the inception of cavitation is given by $K = (-C_p)_{min.}$ is conservative even at very high free stream velocities.

APPENDIX A

Corrections for Tunnel Constraint

For cavitation studies, a quantity which is of primary importance is the value of the minimum pressure on the body immersed in the liquid. When a series of models of the same shape but of different sizes is placed in a water tunnel, the tunnel walls constrict the flow so that the larger bodies experience higher fluid velocities at corresponding points than do the smaller models. This is roughly equivalent to saying that if the tunnel walls were not present, their effect could be replaced by increasing the upstream velocity by an appropriate amount as the size of the model is increased. Of course, the difference between the velocity distribution over an airfoil in a tunnel and that over the same airfoil in an infinite stream varies widely over the chord if the tunnel walls are sufficiently close to the airfoil. Thus, rigorously speaking, one can match the pressures at only one point on the body for both infinite and constrained flow. Accordingly, only the minimum pressures will be matched. It will be further assumed that the position of the minimum pressure on the airfoil is not altered by the presence of the walls.

The required form of the correction factors can now be derived very simply from the Bernoulli equations for the constrained and the infinite flows. If $(\ )_i$ denotes conditions in the infinite or unconstrained flow, and $(\ )_c$ refers the enclosed quantity to conditions in the constrained flow, we have,

for the infinite flow,

$$p_i + \frac{1}{2}\rho V_i^2 = p_{o_i} + \frac{1}{2}\rho V_{o_i}^2 \quad ,$$

and for the constrained flow,

$$p_c + \frac{1}{2}\rho V_c^2 = p_{o_c} + \frac{1}{2}\rho V_{o_c}^2 \quad .$$

The quantities on the left refer to conditions on the body, while those on the right apply to conditions far upstream from the body. If we require that the free stream pressures for both infinite and constrained flows be equal, i.e., $p_{o_c} = p_{o_i}$, the condition that at the minimum pressure point $p_i = p_c$ reduces the two equations above to

$$\left(\frac{V_{o_i}}{V_{o_c}}\right)^2 = \frac{(C_{p_c})_{min.}}{(C_{p_i})_{min.}} \quad .$$

If experimental pressure distributions are at hand, one can then solve for the equivalent free stream velocity in the infinite flow and thus correct the cavitation number,

$$K = \frac{p_o - p_v}{\frac{1}{2}\rho V_o^2} \quad ,$$

to its value for the equivalent infinite stream.

At the time that the major portion of the experimental data were being reduced, experimental pressure distributions were not available. It was therefore necessary to compute the blockage corrections from the theoretical results. Vincenti and Graham[13] have shown that in a closed tunnel of almost any shape, the pressure distribution across the span of a thin airfoil which spans the throat will be constant provided that viscous effects are negligible. They have also shown that if the wake effects are unimportant, it

is possible to replace the working-section diameter, d, of a circular tunnel by an effective two-dimensional height, h_2, given by

$$h_2 = 0.779\, d \qquad \text{(Eq. 41, Ref. 13)} \ .$$

They also show that the total velocity correction with wake effects included can be written in the form

$$\frac{V_{o_i}}{V_{o_c}} = k_1 + 0.321\left(\frac{c}{d}\right) C_d \qquad \text{(Eq. 45, Ref. 13)} \ ,$$

where k_1 is the correction without wake and the term $0.321\,(\frac{c}{d})C_d$ is added to account for the wake. Here, c is the airfoil chord, d is the working-section diameter, and C_d is the drag coefficient of the airfoil as measured in the tunnel. Since no data for the drag of the Joukowski models were available, a value of $C_d = .01$ was assumed.

To obtain the correction factors k_1, the results of Perl and Moses[14] were used. In their work, computations by conformal mapping were made to determine the constriction effects on the velocity distribution over a 12%/o thick airfoil (in addition to other shapes). In their report they present velocity distributions for the airfoil as a function of the parameter tc/h^2 where h is the distance between the bounding walls, and c and t are the airfoil chord and thickness, respectively. Although the section treated by Perl and Moses was not a Joukowski section, it was assumed that at the minimum pressure point the ratios, V_{o_c}/V_{o_i}, for the Joukowski would be equal to those computed from the data presented in Ref. 14. Accordingly, the values of V_{o_c}/V_{o_i} were computed as a function of the given ratios of tc/h^2 and plotted. Then, using the value of h_2 from

Eq. (41), Ref. 13 in place of h, the values of tc/h_2^2 were found for the Joukowski airfoils. The values of V_{o_i}/V_{o_c} without wake effect were taken from the curve derived from Ref. 14. These values of k were used in Eq. (41), Ref. 13, to give the final values of V_{o_i}/V_{o_c}. They were used to compute the corrected values of K and R for all data.

Finally when pressure taps were installed on the models, the correction coefficients were directly computed from faired plots of the pressure distributions over the hydrofoils and a calculated pressure distribution for a Joukowski airfoil in an unlimited stream (Fig. 31). Table IV shows a comparison of the experimentally determined factors with those derived from the reference material as outlined above. The correction factors for the two smaller models show very good agreement, while the factor for the largest model shows that the theoretical value is about 6°/o too high. In view of the large experimental scatter in the data to which these corrections were applied, the portion of the data for which the corrections had already been made prior to the pressure distribution tests was not recorrected.

APPENDIX B

Sound Measuring Equipment

The sound measuring equipment was designed to measure noise intensities in the frequency range of from 20 to 100 kc. The sound sensing element is a Brush C-11 Al hydrophone. Its output is passed through a system of amplifiers and the sound intensity is then read as a voltage.

The hydrophone is placed in an ellipsoidal reflector which serves to focus the sound which originates from the other focus of the ellipsoid on the hydrophone. In order to keep reflection and refraction of the sound waves to a minimum, the reflector hydrophone assembly was submerged in a water-filled tank which was attached to the side of the water tunnel working section. The water was partially de-aerated so as to avoid an accumulation of dissolved air bubbles on the hydrophone and working-section window surfaces. Noise originating at the model was transmitted through a water medium, through the lucite window of the water tunnel test section to the reflecting mirror and then to the hydrophone. Provisions were made on the exterior tank to move the hydrophone mirror assembly to any position in the exterior tank and for adjusting the focus and position of the hydrophone. These features are shown in Fig. 32.

In order to avoid confusion with hydrodynamic pressures the term "sound intensity" has been used rather than the correct name acoustic pressure. Thus "sound intensity" is a measure of acoustic pressure (dynes/cm^2) rather than energy flux.

REFERENCES

1. Plesset, M. S., "The Dynamics of Cavitation Bubbles", Journal of Appl. Mech., Vol. 16, pp. 277-338, Sept. 1949.

2. Reichardt, Reports and Translations No. 776, Ministry of Aircraft Production, (1946); distributed by Office of Naval Research, Navy Department, Washington, D. C.

3. Epstein, P. S., and Plesset, M. S., "On the Stability of Gas Bubbles in Liquid-Gas Solutions", J. Chem. Phys., Vol. 18, No. 11, pp. 1505-1509, Nov. 1950.

4. Zeldovich, Y. B., "Theory of New Phase Formation: Cavitation", Acta Physiocochimica, U.R.S.S., Vol. 28, No. 1, p. 1, 1943.

5. Gilmore, Forrest, "The Dynamics of Condensation and Vaporization", Report No. 21-6 Hydrodynamics Laboratory, Calif. Inst. of Technology, 1951.

6. Gilmore, Forrest, "The Growth or Collapse of a Spherical Bubble in a Viscous Compressible Liquid", Report No. 26-4 Hydrodynamics Laboratory, Calif. Inst. of Technology, April 1, 1952.

7. Gilmore, F. R., and Plesset, M. S., "Scaling Laws for Incipient Cavitation Noise", Report No. 26-1, Hydrodynamics Laboratory, Calif. Inst. of Technology, April 3, 1950.

8. Noltingk, B. E. and Neppiras, E. A., "Cavitation Produced by Ultrasonics", Proc. Phys. Soc. of London, Vol. 63, Sec. B, p. 674, 1950.

9. Rattray, Maurice, Jr., "Perturbation Effects in Bubble Dynamics", Report No. 21-5, Hydrodynamics Laboratory, Calif. Inst. of Technology, Jan. 1951.

10. Birkhoff, Garrett, "Hydrodynamics", Princeton Univ. Press, p. 106, 1950.

11. Gutsche, F., "Hydrodynamishe Probleme Des Schiffsantriebs", Editors G. Kempf and E. Foerster, printed by Freunde and Förderer of Hamburg for the Hamburg Towing Tank, 1932.

12. Knapp, R. T., Levy, J., O'Neill, J. P., and Brown, F. B., "The Hydrodynamics Laboratory of the California Institute of Technology", Trans. A.S.M.E., p. 437, July 1948.

13. Vincenti, W. G., and Graham, D. J., "The Effect of Wall Interference Upon the Aerodynamic Characteristics of an Airfoil Spanning a Closed-Throat Circular Wind Tunnel", NACA T.R. 849, 1946.

14. Perl, W., and Moses, H. E., "Velocity Distributions on Symmetrical Airfoils in Closed Tunnels by Conformal Mapping", NACA T.N. 1642, 1948.

15. Daily, J. W., "Force and Cavitation Characteristics of the NACA 4412 Hydrofoil", Report ND-19, Hydrodynamics Laboratory, Calif. Inst. of Technology, June 1944. Subsequently published as: "Cavitation Characteristics and Infinite Aspect Ratio Characteristics of a Hydrofoil Section", Trans. Amer. Soc. Mech. Engrs. 71, 269-284 (Apr. 1949).

16. Knapp, R. T., and Hollander, A., "Laboratory Investigations of the Mechanism of Cavitation", Trans. ASME, p. 419, July 1948.

17. Rouse, Hunter, and McNown, J. S., "Cavitation and Pressure Distribution", and "Head Forms at Zero Angle of Yaw", State Univ. of Iowa, Studies in Engineering, Bulletin 32, p. 12, 1948.

18. Eisenburg, P., "On the Mechanism and Prevention of Cavitation (1950). David W. Taylor M del Basin Report 712.

19. Plesset, M. S., "Rate of Formation of Vapor in a Uniformly Heated Liquid". (1949). North American Aviation, Inc. Special Research Report NAA-SR-53.

20. Epstein, P. S., "Textbook of Thermodynamics". John Wiley and Sons, Inc. (1937). Ch. IX. p. 159.

TABLE I - SUMMARY OF NACA 4412 HYDROFOIL EXPERIMENTAL DATA
(taken from bubble histories such as Fig. 6)

Bubble Number	Free Stream Velocity fps	Reynolds Number Millions	Cavitation Number	Max. Bubble Dimension Ft.	Max. Bubble Eccentricity Major Dia./ Minor Dia.
Angle of Incidence, $\alpha = 0^\circ$					
65-1	34.9	.87	0.59	12.2	1.36
65-2	34.9	.87	0.59	6.8	2.0
66-1	34.9	.87	0.56	14.7	1.8
66-2	34.9	.87	0.56	7.0	1.8
67-1	40.4	1.01	0.65	4.8	2.15
68-1	40.8	1.02	0.58	9.9	2.0?
68-2	40.8	1.02	0.58	2.6	1.50
71-1	51.7	1.29	0.59	12.4	1.45
71-2	51.7	1.29	0.59	7.5	1.75
72-1	51.7	1.29	0.57	5.?	1.45
73-1	40.7	1.02	0.56	13.6	1.3?
74-1	40.4	1.01	0.54	5.7	1.55
75-1	51.7	1.29	0.57	4.1	1.55
Angle of Incidence, $\alpha = +4^\circ$					
77-1	34.6	0.87	1.02	9.9	1.70
78-1	34.8	0.87	1.02	10.2	2.14
79-1	34.6	0.87	0.76	11.6	1.83
80-1	34.7	0.87	1.06	3.6	2.29
80-2	34.7	0.87	1.06	8.6	1.67
81-1	40.2	1.01	1.79	7.3	1.72
82-1	40.2	1.01	0.98	8.6	1.71
83-1	40.3	1.01	0.96	11.4	1.32
84-1	40.5	1.01	0.93	11.3	1.53
Angle of Incidence, $\alpha = -4^\circ$					
85-1	35.0	0.88	0.62	8.9	1.48
86-1	35.0	0.88	0.53	3.5	1.29
86-2	35.0	0.88	0.53	7.6	1.46
88-1	35.0	0.88	0.56	3.5	1.43
90-1	41.0	1.03	0.54	4.7	1.59
91-1	40.7	1.02	0.46	9.4	1.?9
92-1	40.8	1.02	0.51	4.2	1.35
92-2	40.8	1.02	0.51	5.0	2.1
94-1	52.4	1.31	0.80	3.9	1.37
95-1	52.2	1.31	0.79	3.4	1.27
95-2	52.2	1.31	0.79	9.0	1.35
96-1	52.1	1.30	0.43	9.8	1.45
96-2	52.1	1.30	0.43	14.2	1.29
97-1	52.2	1.31	0.44	11.1	1.42
97-2	52.2	1.31	0.44	6.5	2.12
98-1	52.5	1.31	0.46	5.9	1.31
98-2	52.5	1.31	0.46	10.7	1.30

TABLE II - AVERAGE MAXIMUM BUBBLE SIZE VS. THE ANGLE OF INCIDENCE, α

Free stream velocity 40 fps

Angle of Incidence α	Average Cavitation Number $\bar{K}$	Minimum Pressure Coefficient $(C_p)_{min.}$	Average Max. Bubble Dimension mm.
-4°	0.51	-0.40	7.2
0°	0.58	-0.58	7.8
$+4^\circ$	1.14	-0.93	12.8

TABLE III - SUMMARY OF BUBBLE HISTORY DATA OVER THE JOUKOWSKI HYDROFOILS
(from curves such as Fig. 8)

Free stream velocity 40 fps.
Data uncorrected for wall effect.

Bubble No.	Max. Bubble Dimension in fraction of chord length c, (T/c) max.
Chord length, c = 2"	
Cavitation No. K = 0.26	
2-1	0.22
2-2	0.12
2-3	0.23
2-4	0.25
2-5	0.25
2-6	0.22
2-7	0.20
2-8	0.20
2-9	0.21
2-11	0.21
2-12	0.18
Cavitation No. K = 0.27	
3-1	0.18
3-2	0.25
3-3	0.23
3-4	0.21

Bubble No.	Max. Bubble Dimension in fraction of chord length c, (T/c) max.
Chord length, c = 4"	
Cavitation No. K = 0.25	
4-1	0.30
4-2	0.11
4-3A	0.26
4-4	0.18
4-5	0.28
4-6	0.25
4-7	0.20
4-8	0.18
4-9	0.16
4-10	0.05
4-11	0.13
4-12A	0.18
4-12B	0.15
4-12C	0.07

Bubble No.	Max. Bubble Dimension in fraction of chord length c, (T/c) max.
Chord length, c = 4"	
Cavitation No. K = 0.26	
5-1A	0.18
5-1B	0.16
5-2	0.19
5-3A	0.13
5-3B	0.25
5-4A	0.19
5-4B	0.25
5-5	0.06
5-6	0.06
5-7	0.17
5-8	0.23
5-9	0.16
5-10	0.16
5-11	0.19
5-13	0.22
5-14	0.50

TABLE III - Continued

Free stream velocity 40 fps.
Data uncorrected for wall effect.

Bubble No.	Max. Bubble Dimension in fraction of chord length c, (T/c) max.
Chord length, c = 8"	
Cavitation No. K = 0.35	
6-1	0.11
6-2	0.11
6-3	0.10
6-4	0.23
6-5	0.16
6-6	0.09

Bubble No.	Max. Bubble Dimension in fraction of chord length c, (T/c) max.
Chord length, c = 8"	
Cavitation No. K = 0.24	
7-1A	0.15
7-1B	0.08
7-1C	0.16
7-2	0.23
7-3	0.10
7-5	0.07
7-6A	0.12
7-6B	0.07
7-8A	0.18
7-8B	0.14
7-8C	0.06
7-9A	0.14
7-9B	0.13
7-9C	0.06

Bubble No.	Max. Bubble Dimension in fraction of chord length c, (T/c) max.
Chord length, c = 8"	
Cavitation No. K = 0.24	
7-10A	0.17
7-10B	0.20
7-10C	0.15
7-12A	0.13
7-12B	0.19
7-12C	0.14
7-13A	0.17
7-13B	0.06
7-14A	0.20
7-14B	0.17
7-15	0.08
7-16	0.09
7-17	0.23

TABLE IV - COMPARISON OF THEORETICAL AND EXPERIMENTAL WALL CORRECTIONS

Model Chord Inches	Correction Factor $(V_{c_c}/V_{c_i})^2$ Derived from Theory Refs. 7 and 8	Correction Factor $(V_{c_c}/V_{c_i})^2$ Experimental Values
8	1.19	1.12
4	1.06	1.08
2	1.01	1.04

TABLE V - TIME REQUIRED FOR A BUBBLE GROWTH, R/R_o, OF 492.75 FROM THE I.B.M. DIGITAL COMPUTER

γ, Bubble Air Content Parameter.	α, Bubble Driving Parameter. DIMENSIONLESS TIME, τ.														α_c for $\tau \rightarrow \infty$ for the given values of γ.
	.145	.150	.155	.160	.165	.170	.175	.180	.185	.190	.200	.210	.220	.230	
0										1474.6	1424.6	1382.6	1345.3	1311.4	.1807
.2									1491.9	1465.1	1418.8	1378.2	1341.7	1308.3	.1754
.4							1544.1	1511.8	1484.2	1459.4	1414.8	1375.1	1339.1	1306.2	.1696
.6						1567.1	1533.6	1505.0	1479.2	1455.3	1411.8	1372.7	1337.1	1304.4	.1641
.8					1592.4	1557.2	1527.3	1500.3	1475.4	1452.1	1409.4	1370.7	1335.5	1303.0	.1593
1.0					1582.6	1551.1	1522.8	1496.7	1472.4	1449.5	1407.3	1369.1	1334.0	1301.7	.1550
1.2				1609.9	1576.4	1546.6	1519.3	1493.8	1469.9	1447.4	1405.6	1367.6	1332.8	1300.6	.1509
1.4			1639.3	1603.5	1572.0	1543.2	1516.5	1491.4	1467.8	1445.5	1404.1	1366.3	1331.7	1299.6	.1470
1.6		1671.2	1632.6	1599.0	1568.5	1540.4	1514.1	1489.4	1466.0	1443.9	1402.7	1365.2	1330.6	1298.7	.1430
1.8	1706.1	1663.7	1627.7	1595.3	1565.6	1538.0	1512.0	1487.6	1464.4	1442.4	1401.5	1364.1	1329.7	1297.9	.1394

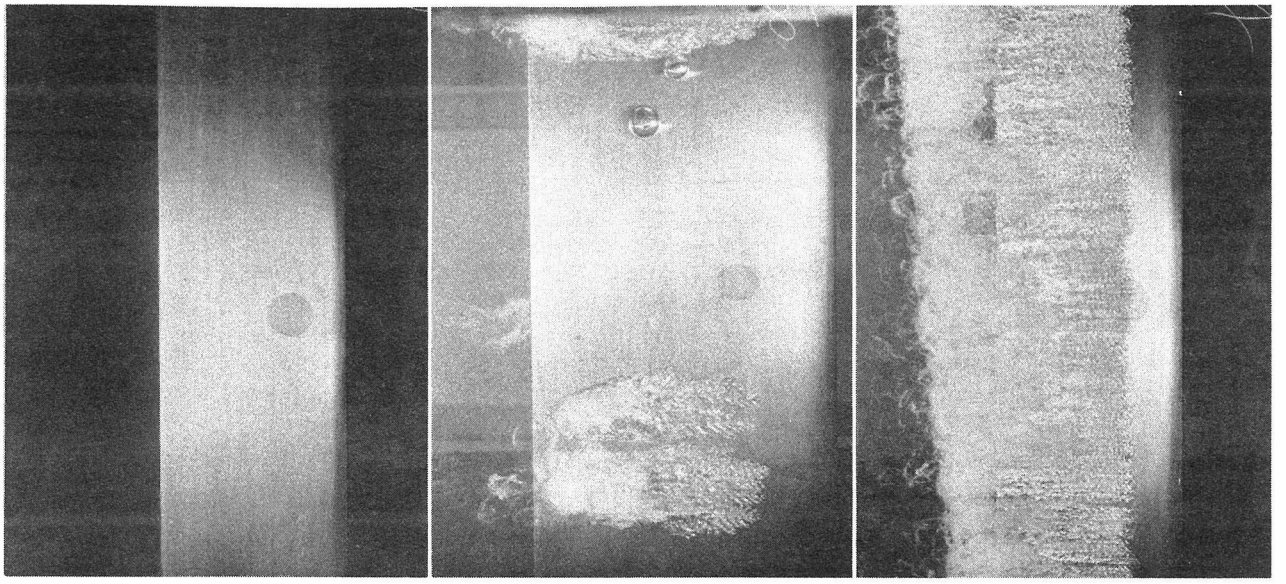

Fig. 1 - Three regimes of liquid flow

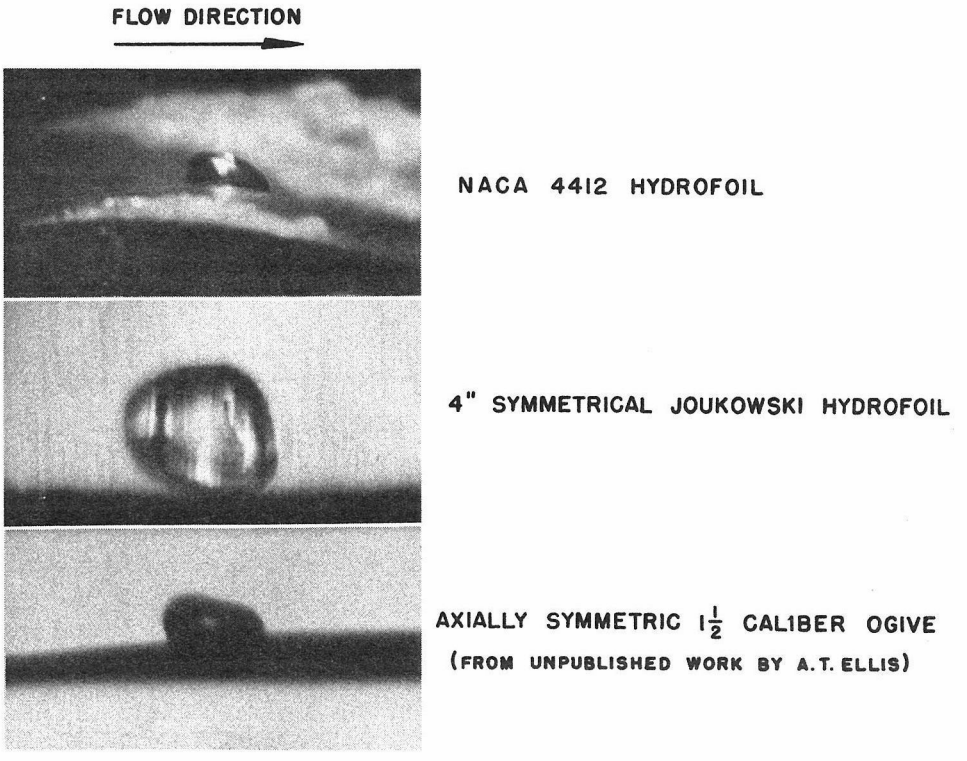

Fig. 2 - Examples of bubble asymmetries

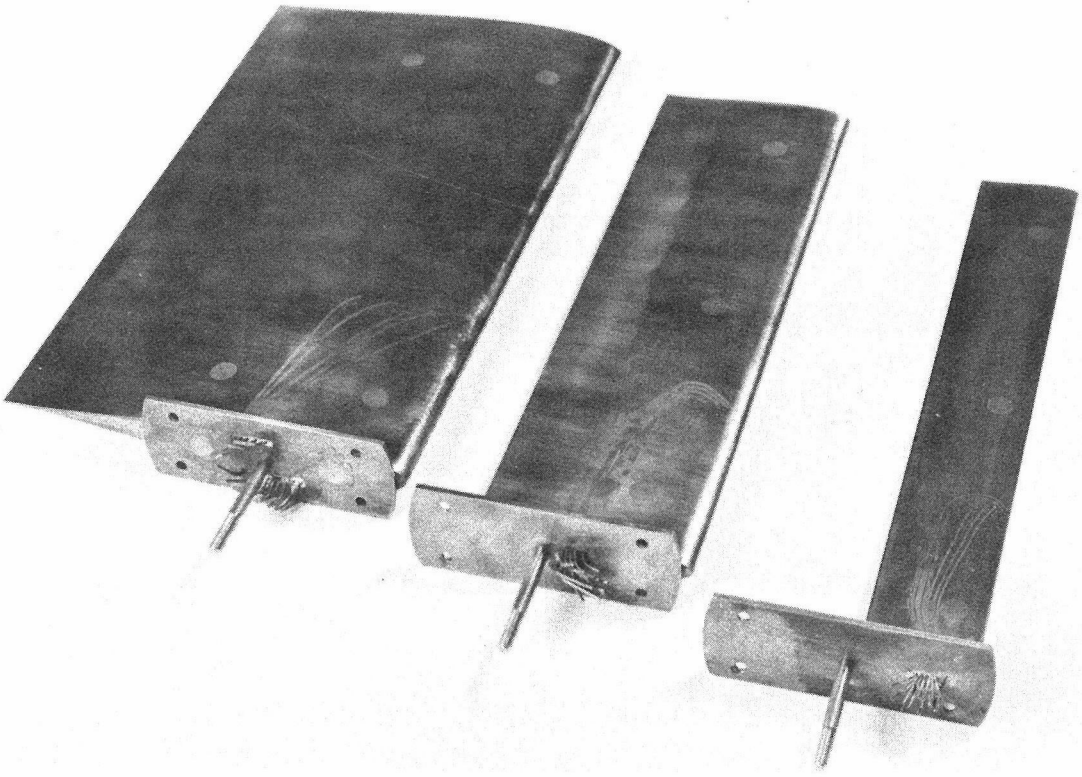

Fig. 3 - Photograph of the three Joukowski hydrofoils

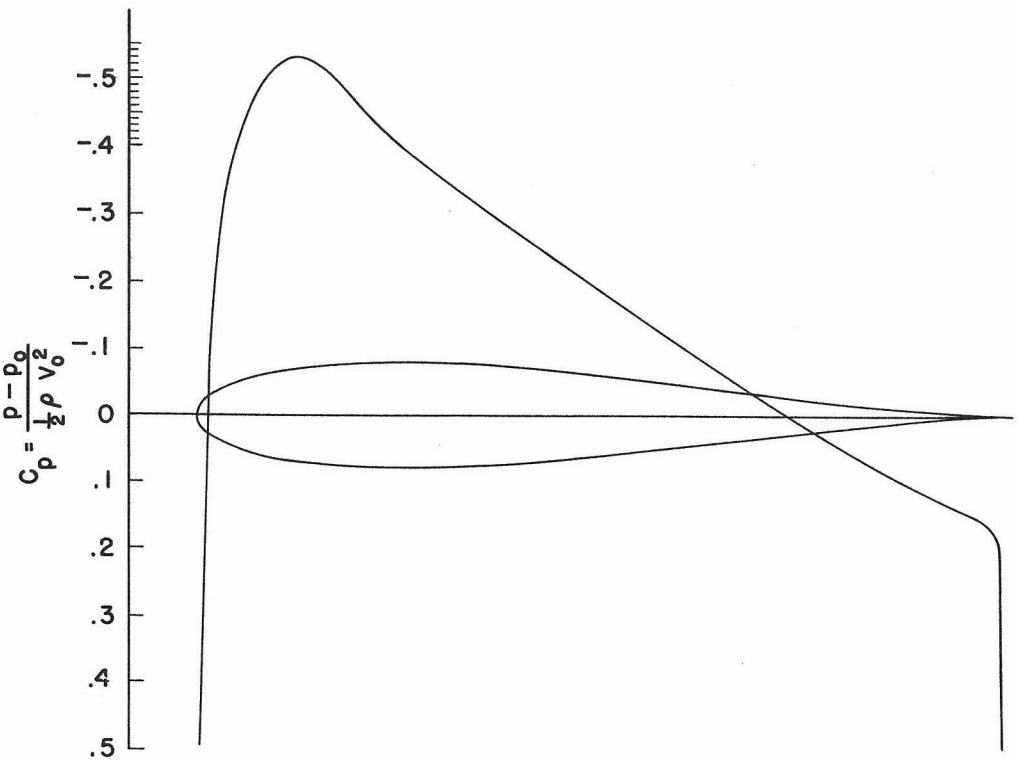

Fig. 4 - The Joukowski airfoil section and its theoretical pressure distribution at zero angle of attack

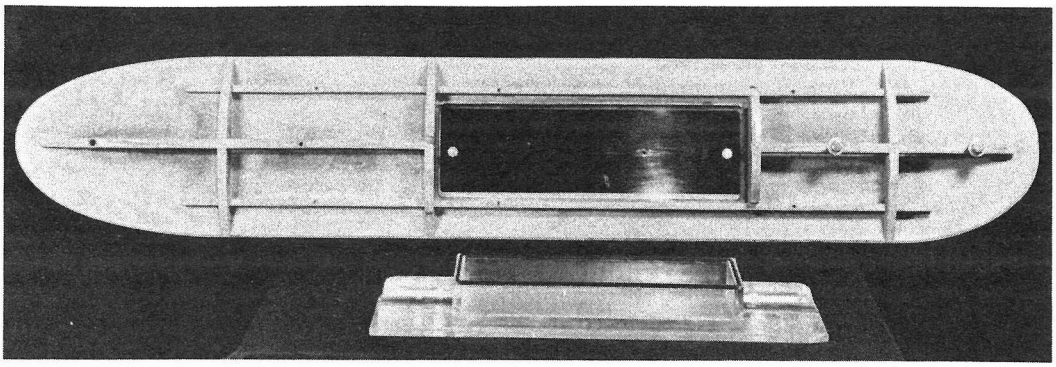

UPPER SIDE PLATE AND WINDOW ASSEMBLY

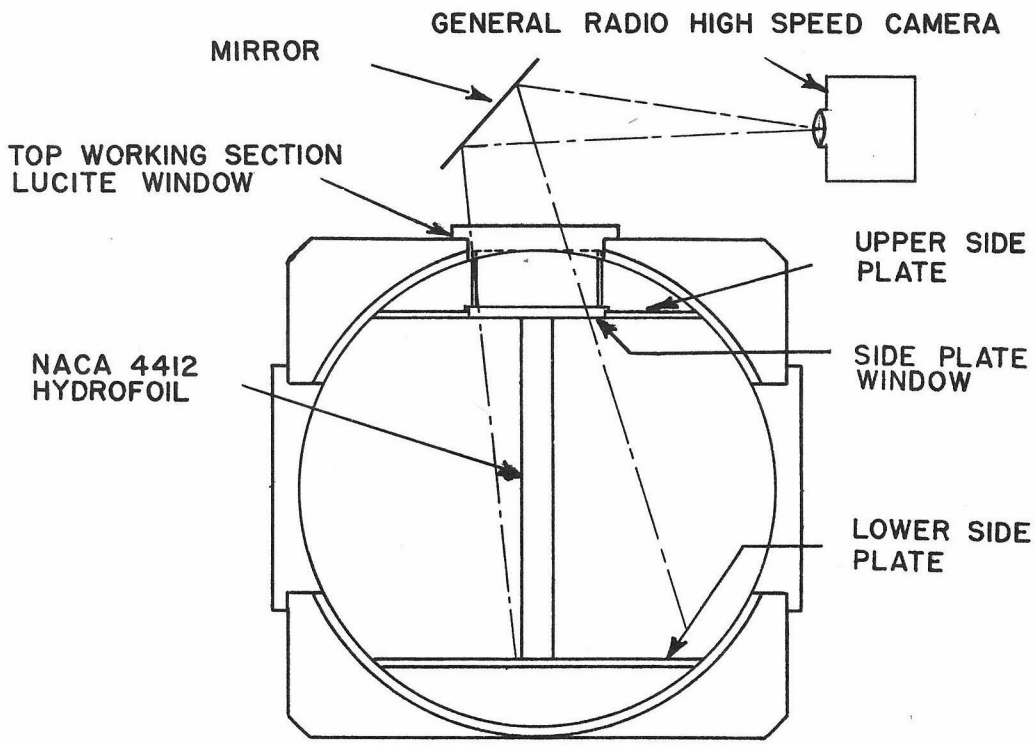

SCHEMATIC VIEW OF TEST SET-UP IN HIGH SPEED WATER TUNNEL
WORKING SECTION (LOOKING DOWNSTREAM)

Fig. 5 - NACA 4412 hydrofoil test arrangement

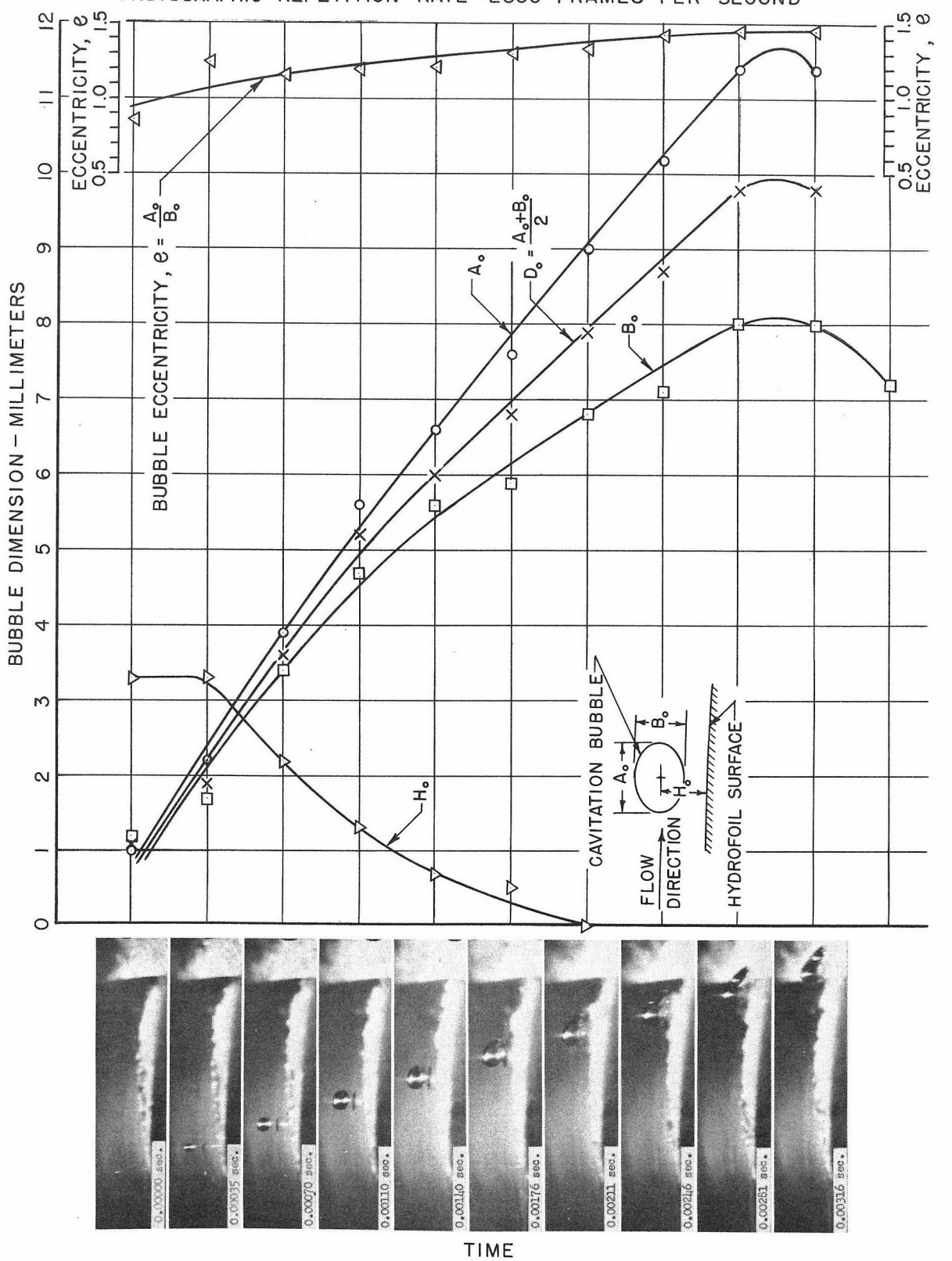

Fig. 6 - Growth of a cavitation bubble over the upper surface of the NACA 4412 hydrofoil

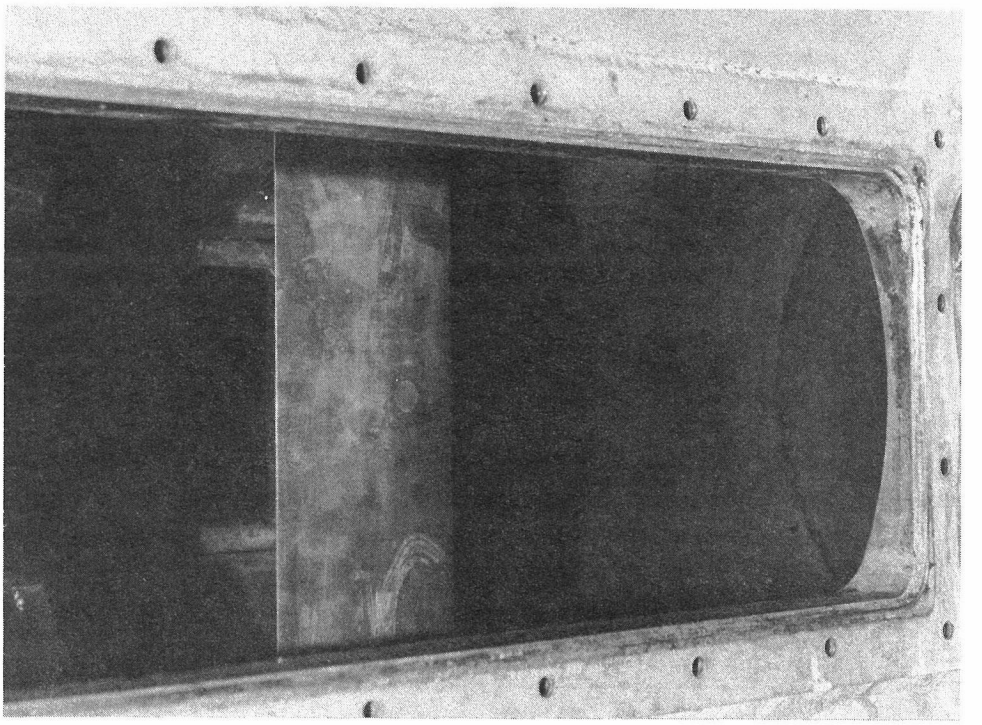

PHOTOGRAPH OF THE 4-IN JOUKOWSKI MODEL INSTALLED IN THE WORKING SECTION OF THE HIGH SPEED WATER TUNNEL

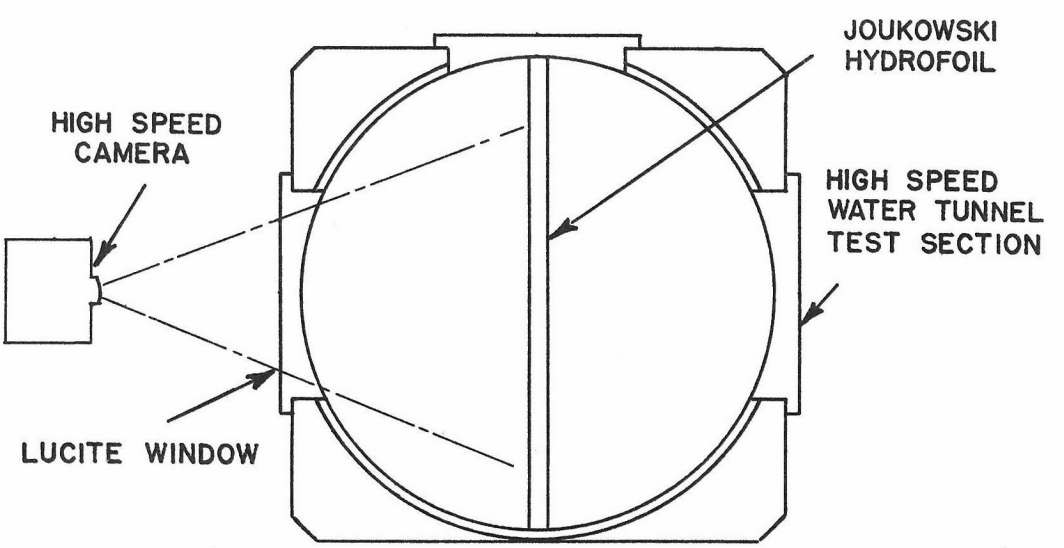

SCHEMATIC VIEW (LOOKING DOWNSTREAM) OF TEST SET-UP

Fig. 7 - Joukowski hydrofoil test arrangement

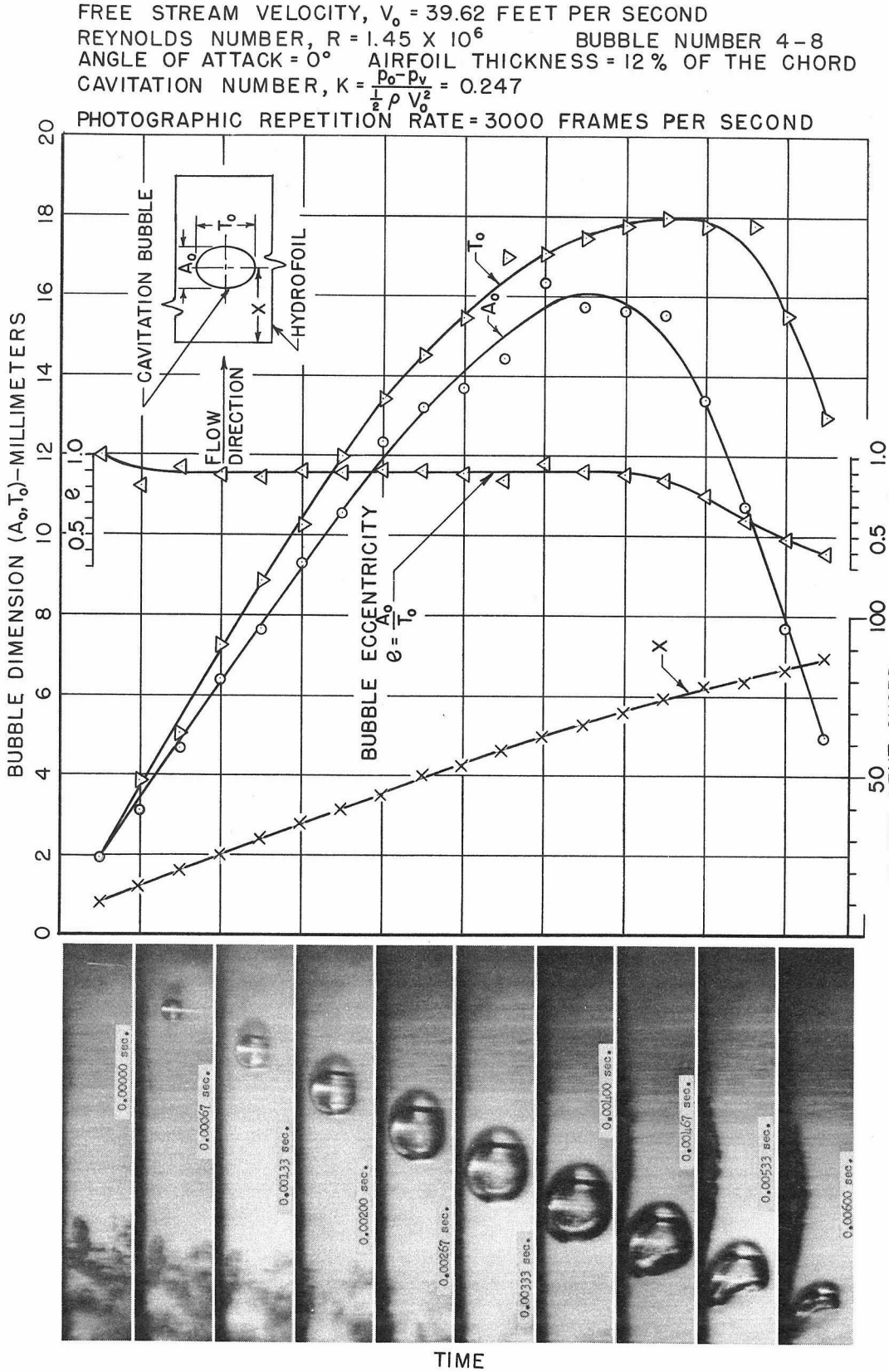

Fig. 8 - A cavitation bubble growing on the 4-inch chord symmetrical Joukowski hydrofoil

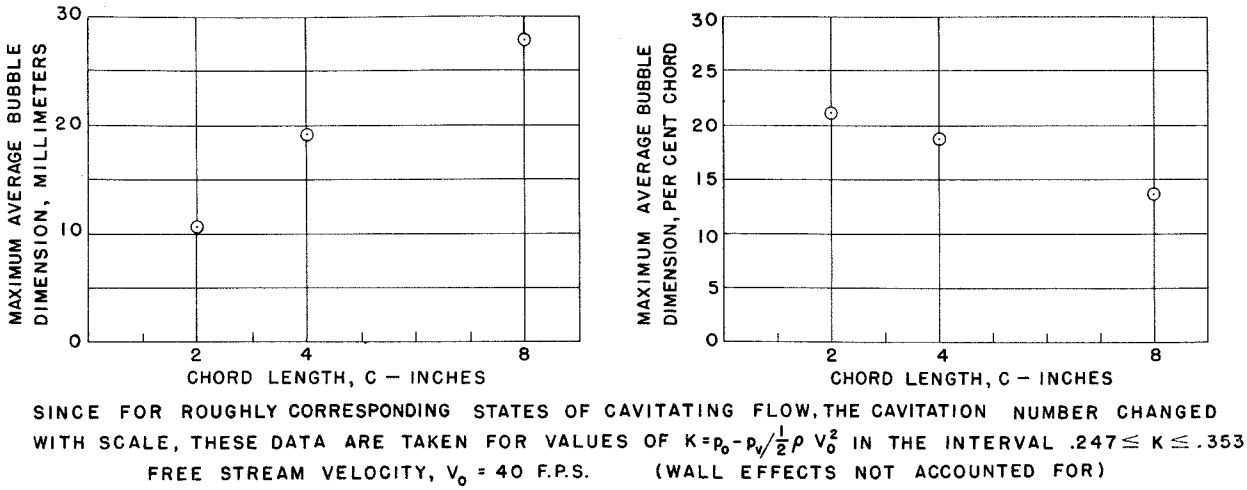

Fig. 9 - Experimental verification of the dependence of maximum bubble size on body scales

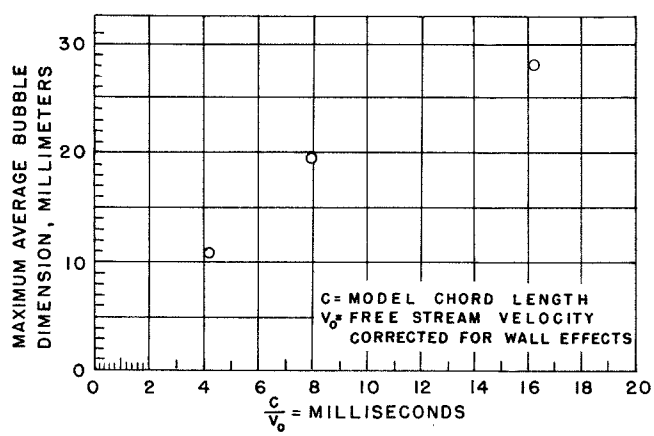

Fig. 10 - Maximum bubble dimension versus c/V_o

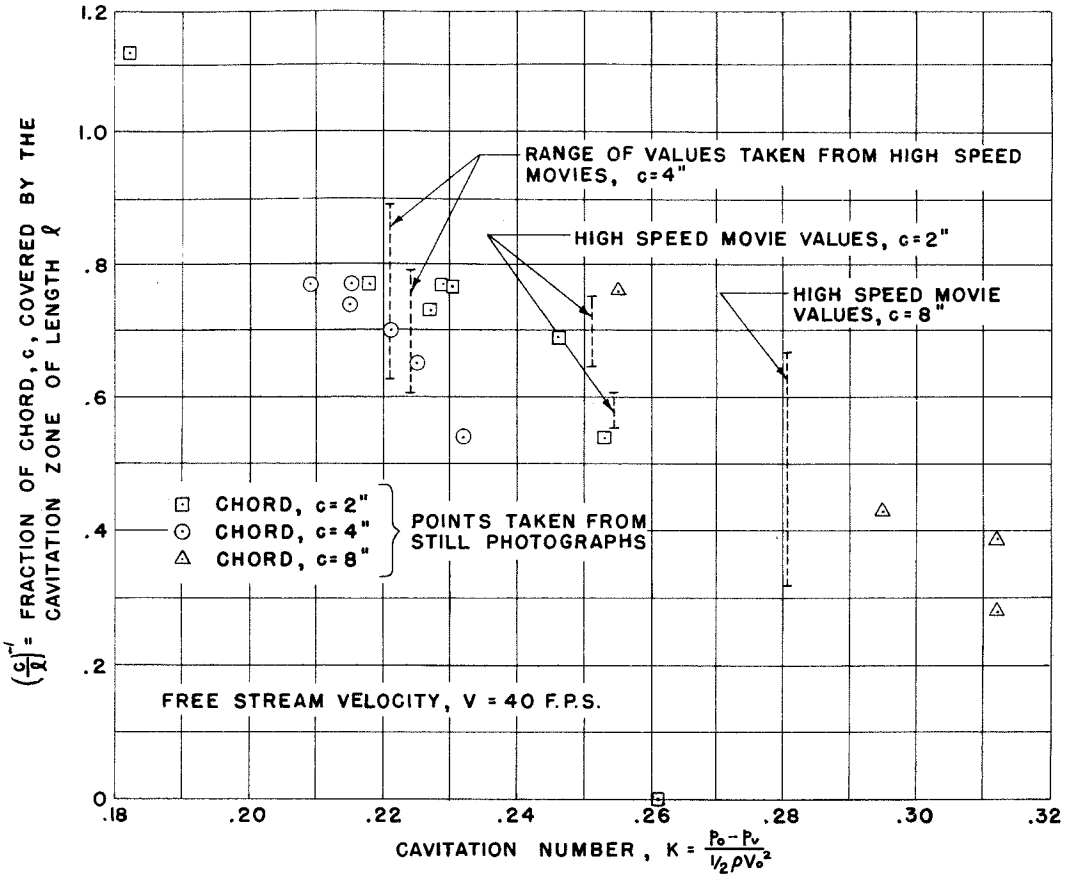

Fig. 11 - Nonsimilarity of the zone of cavitation on different sized models

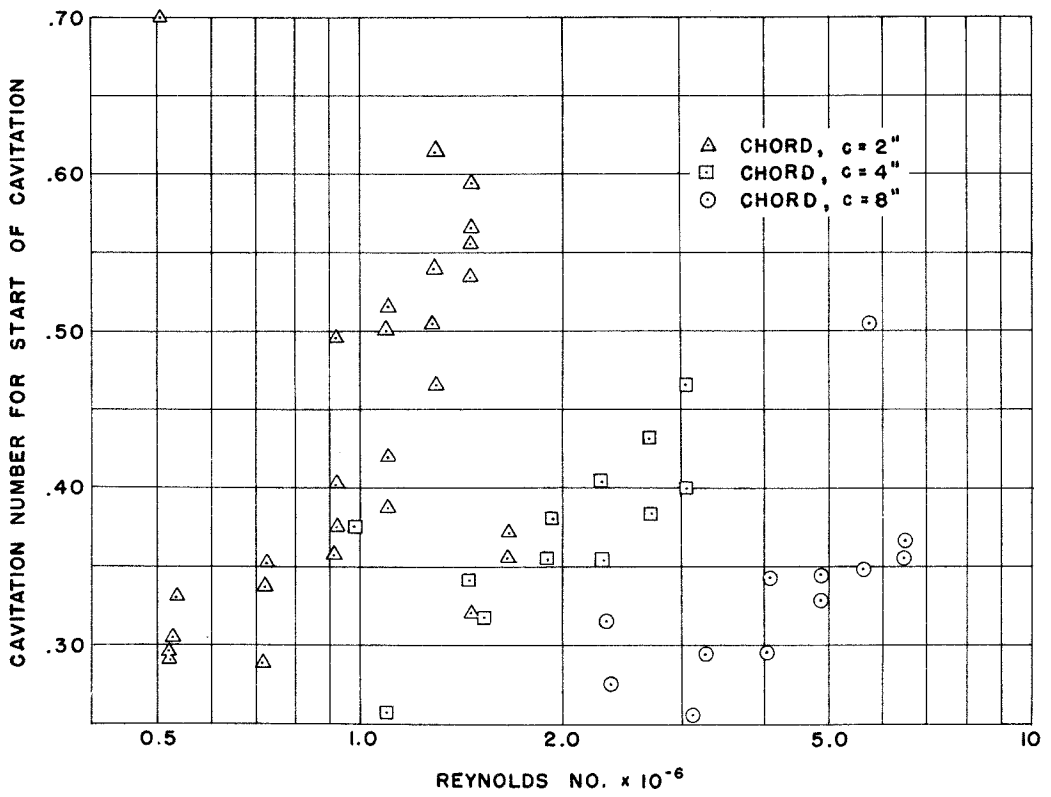

Fig. 12 - The cavitation number, K, for incipient cavitation vs. the Reynolds number, R, for the Joukowski hydrofoils

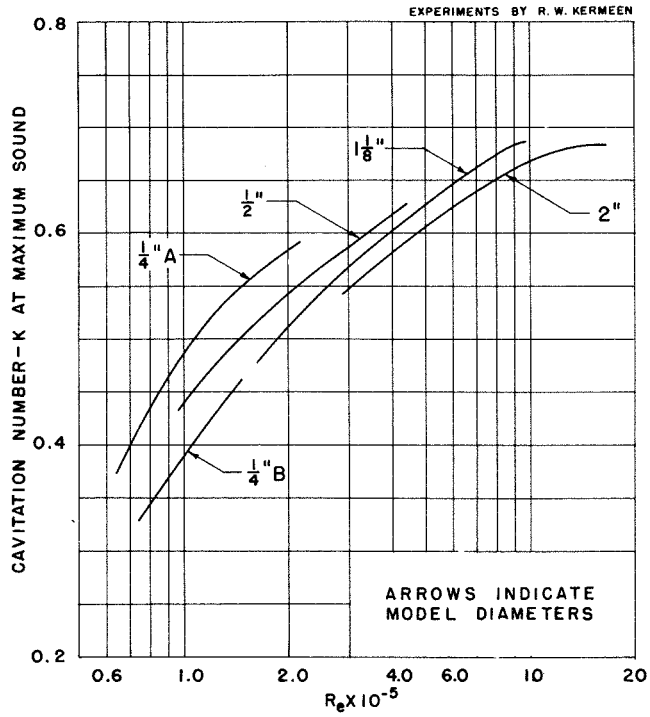

Fig. 13 - The cavitation number, K, for incipient cavitation vs. the Reynolds number, R, for hemisphere-nosed bodies

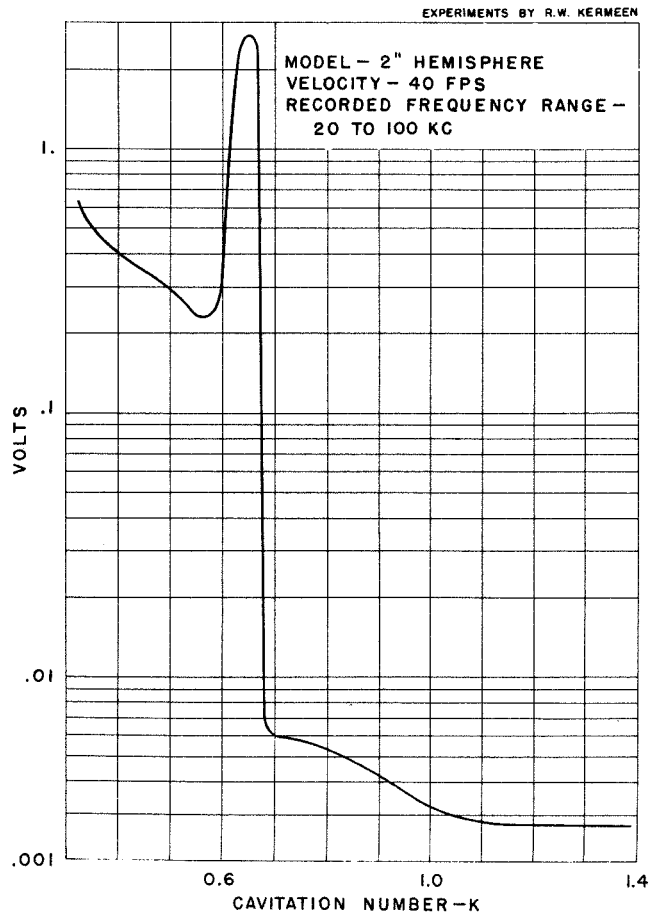

Fig. 14 - Typical sound curve for a hemisphere-nosed body

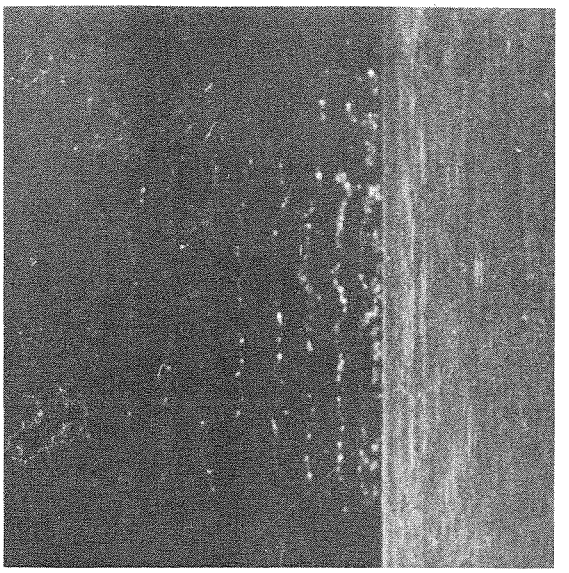

Fig. 15 - Bands of cavitation downstream from the trailing edge of a singing Joukowski hydrofoil

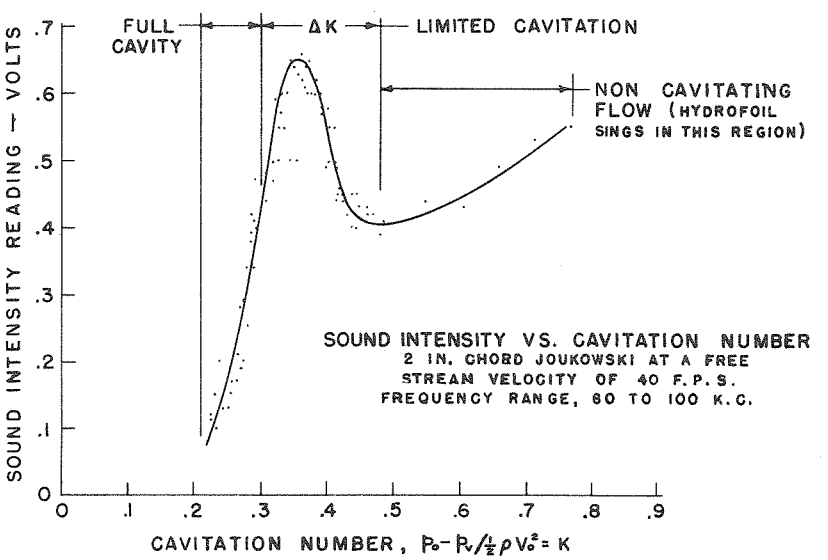

Fig. 16 - Typical sound curve for a Joukowski hydrofoil

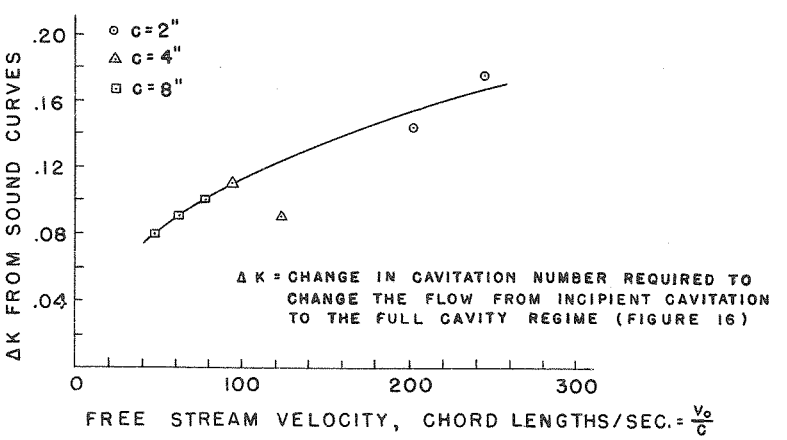

Fig. 17 - Limited cavitation flow regime for the Joukowski hydrofoils

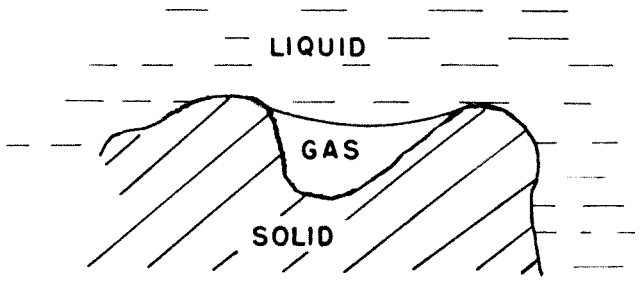

Fig. 18 - A stable three phase cavitation nucleus

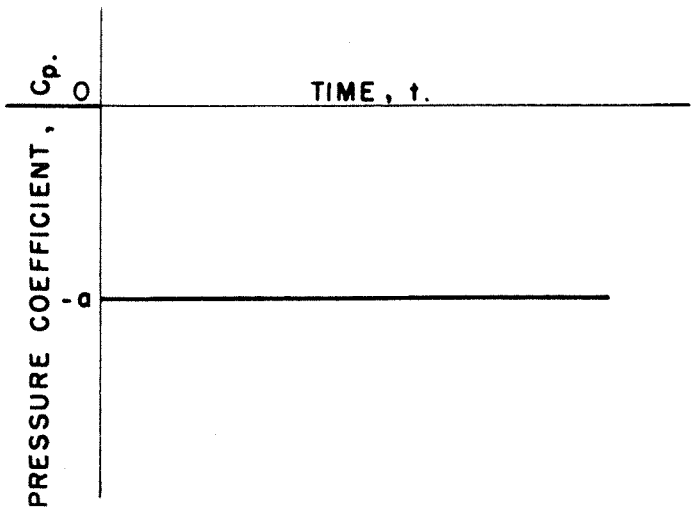

Fig. 19 - The step function pressure law

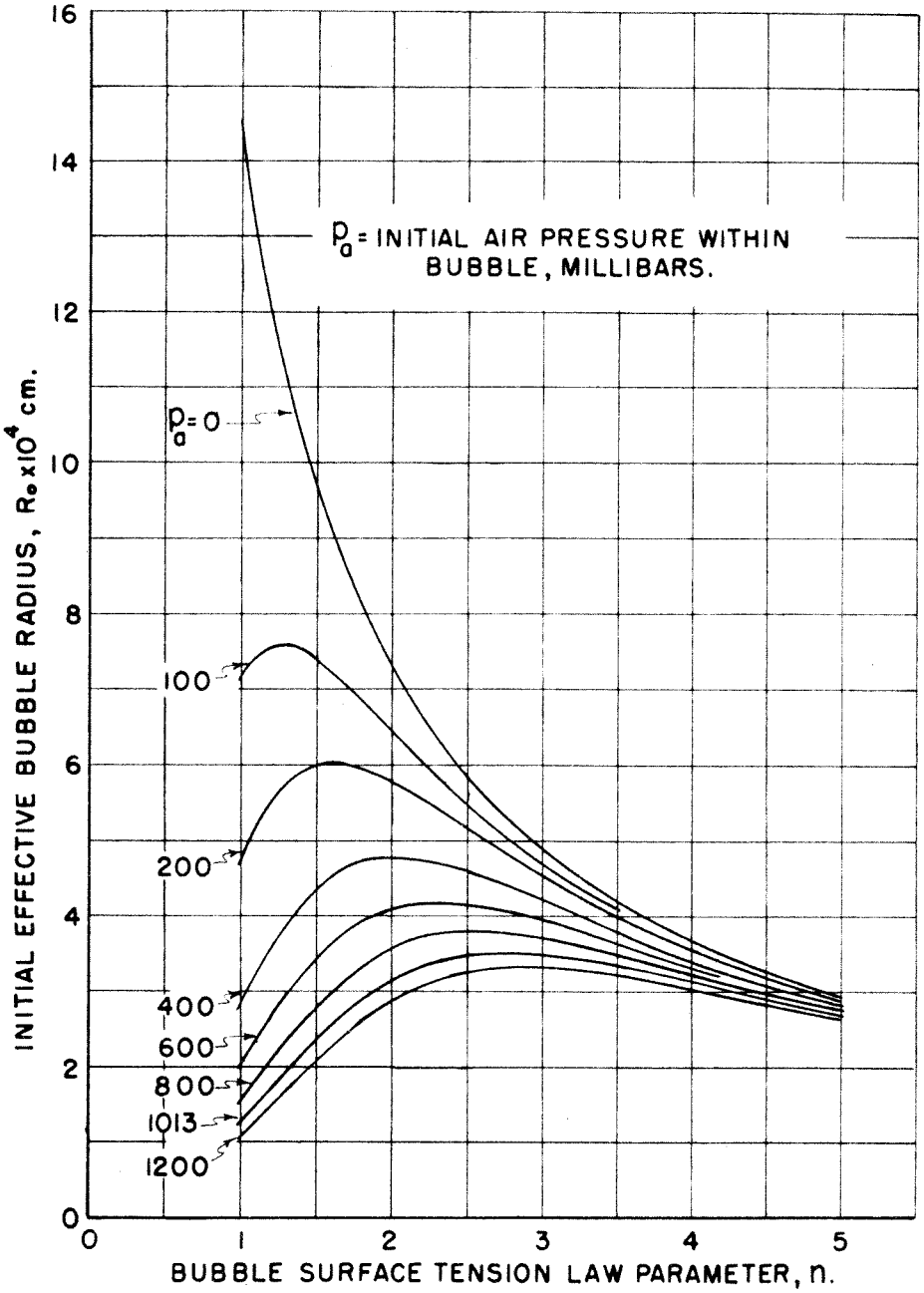

Fig. 20 - Estimates for the initial effective bubble radius under various dissolved air and surface tension law conditions

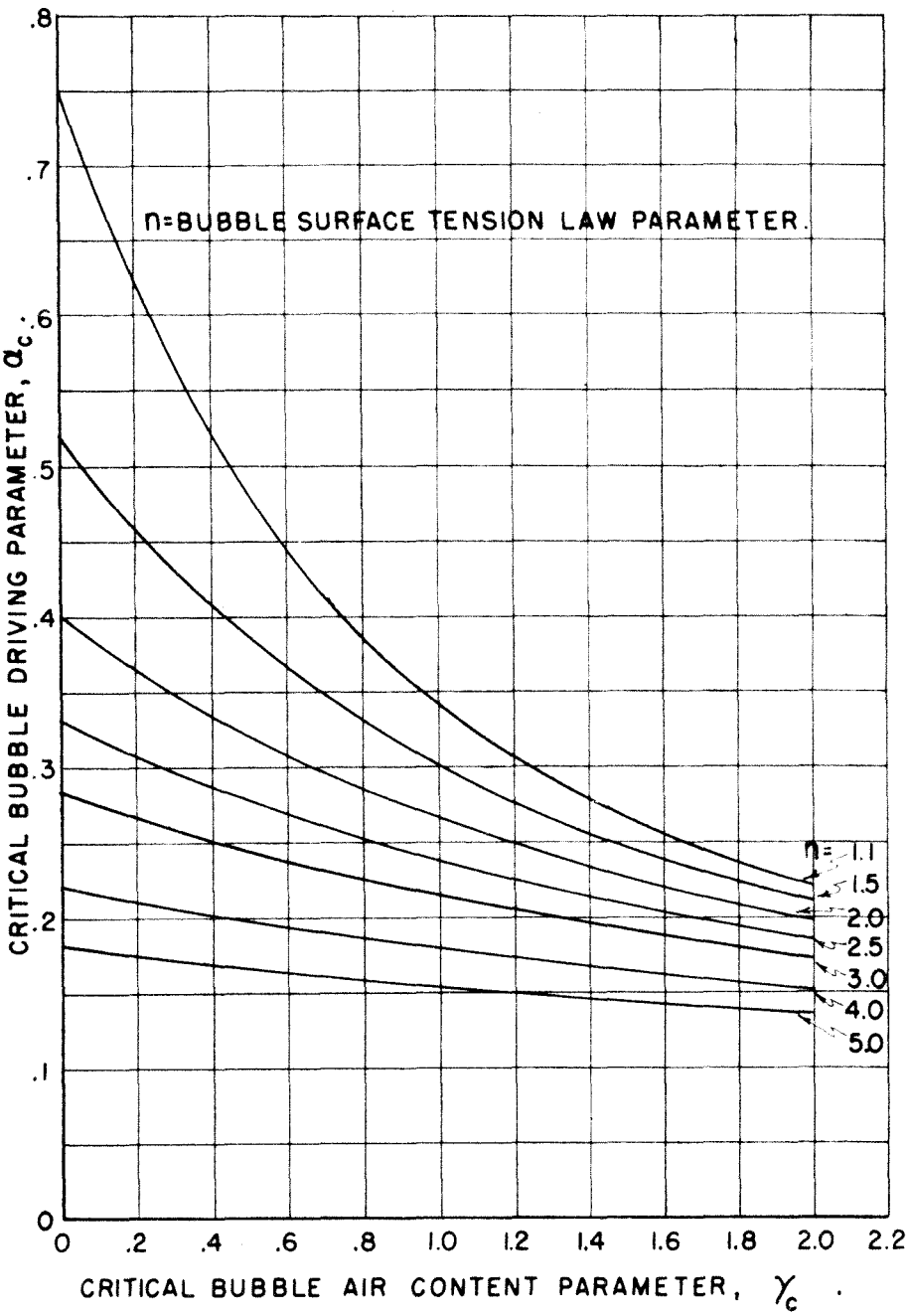

Fig. 22 - The critical conditions for the occurrence of cavitation

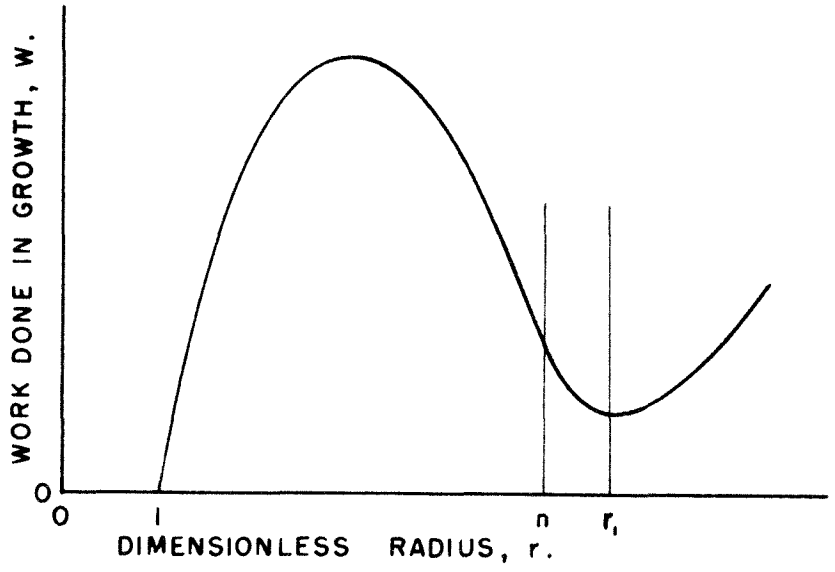

Fig. 21 - Schematic variation of the work done by the bubble in its growth under the step function pressure law

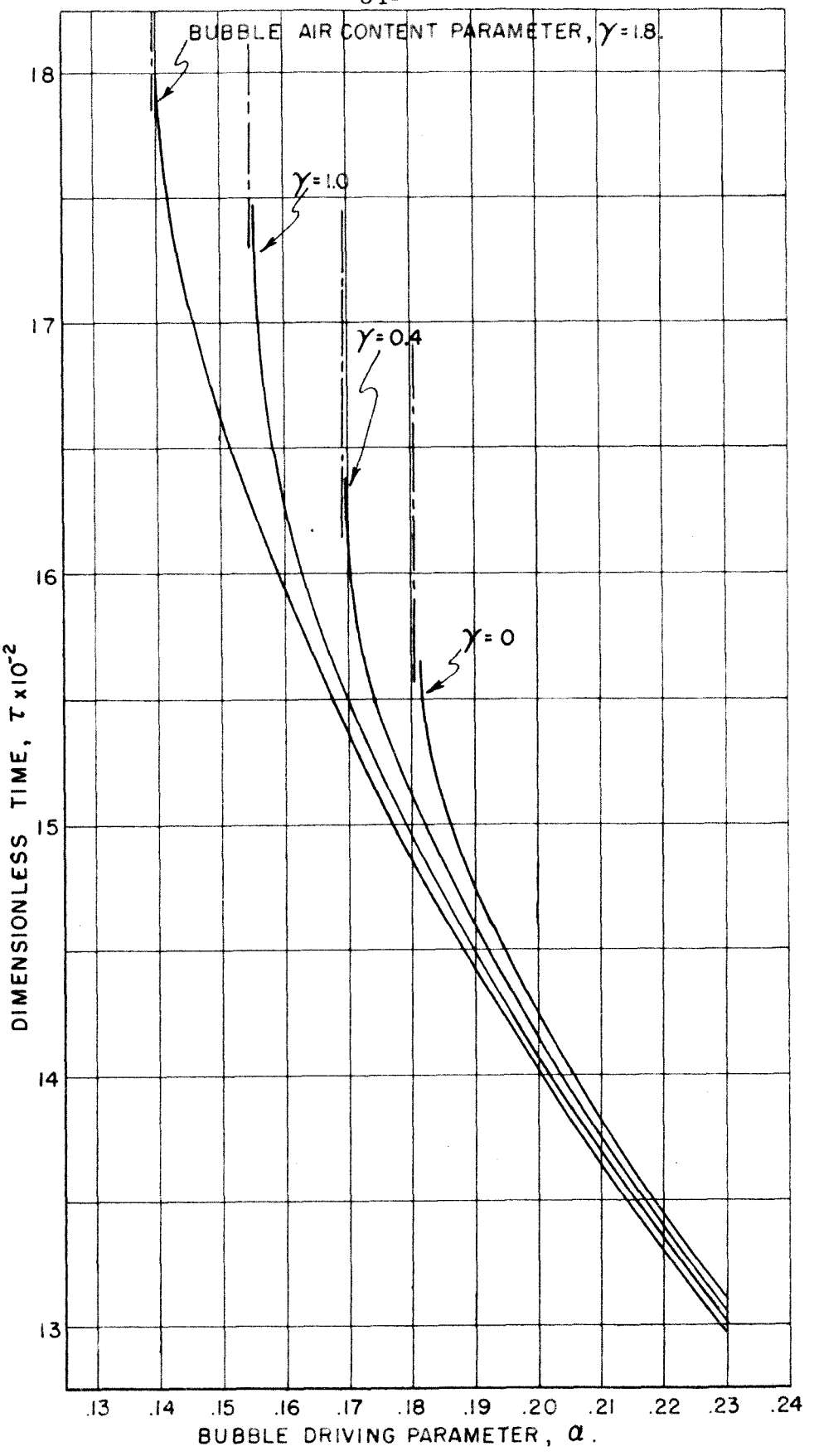

Fig. 23 - Graph of the function $\tau = F(\alpha, \gamma)$

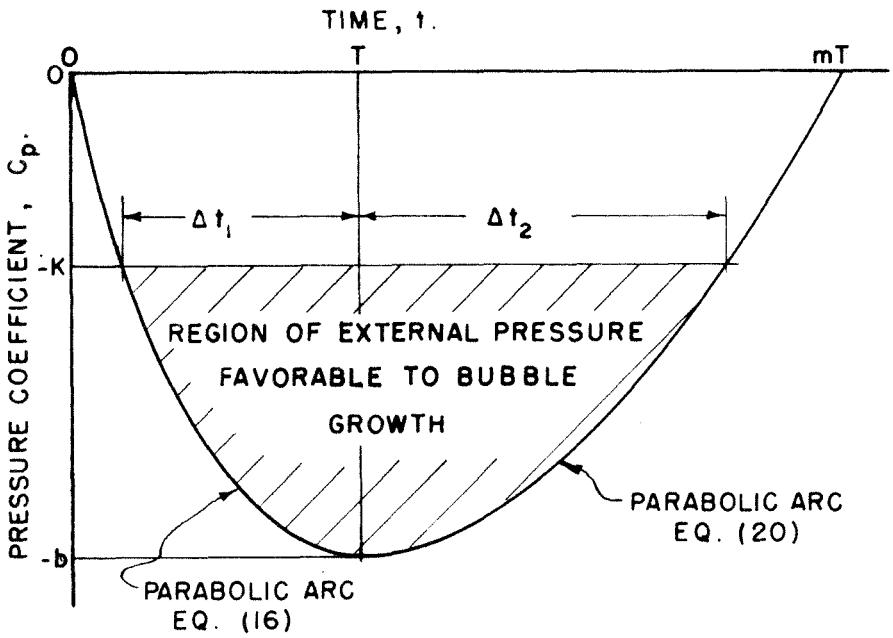

Fig. 24- The time-parabolic pressure law

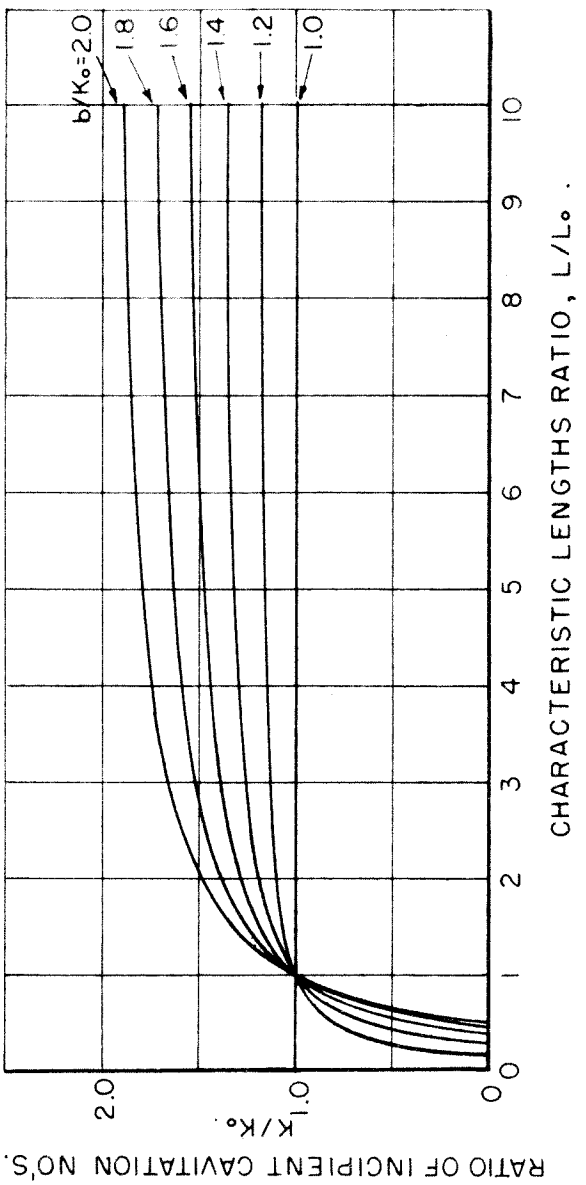

Fig. 25 - The scaling condition for incipient cavitation for very large free stream velocities ($V_o \longrightarrow \infty$)

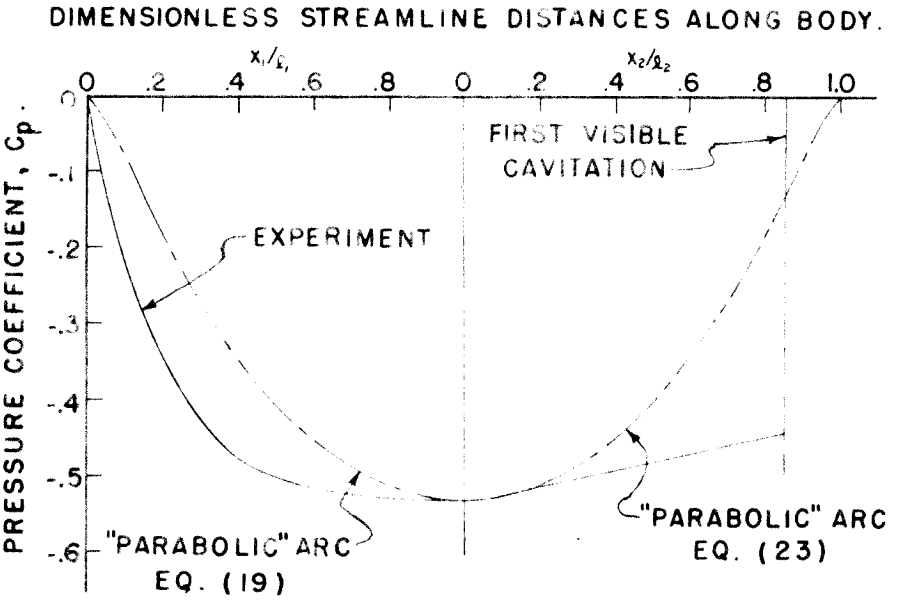

Fig. 26 - Comparison of the experimental pressure distribution with the parabola-like spatial pressure distribution for the Joukowski hydrofoils

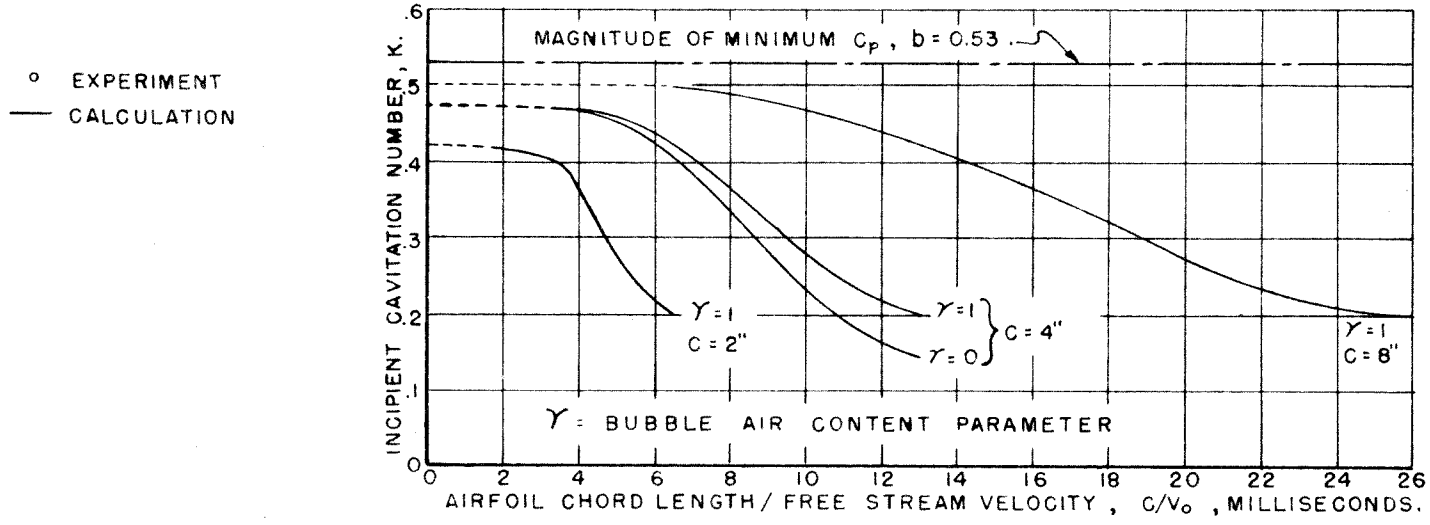

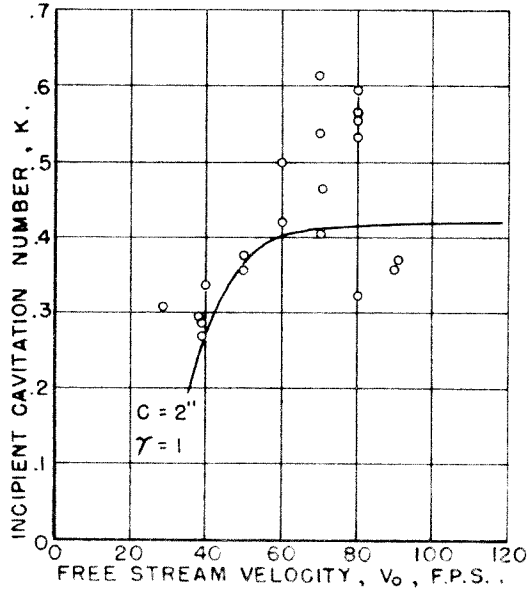

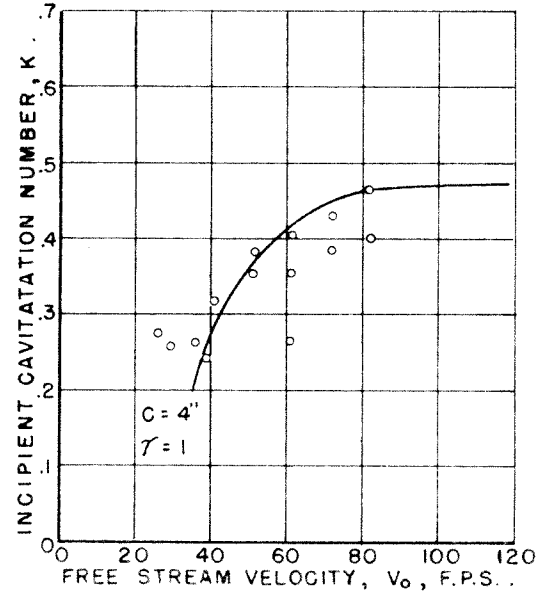

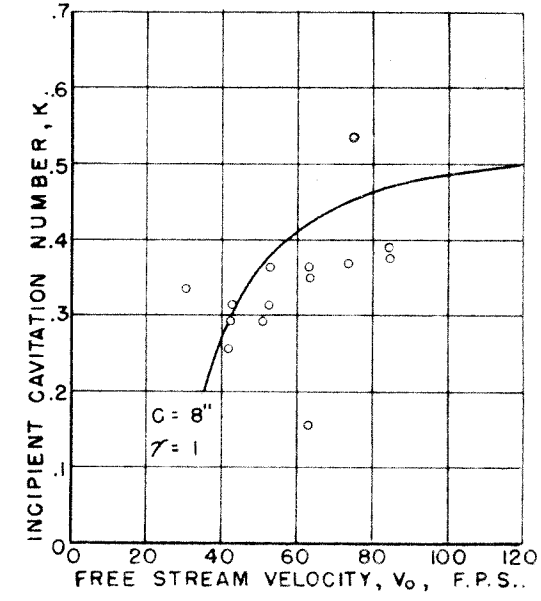

Fig. 27 - Calculated and experimental results for incipient cavitation on the Joukowski Hydrofoils

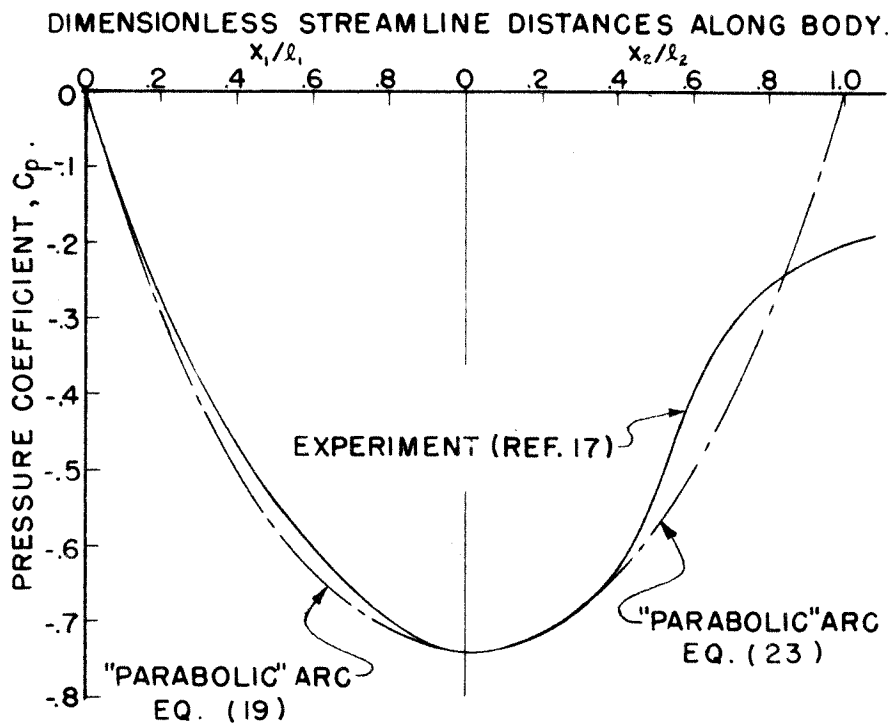

Fig. 28 - Comparison of the experimental pressure distribution with the parabola-like spatial pressure distribution for the "Hemisphere" models

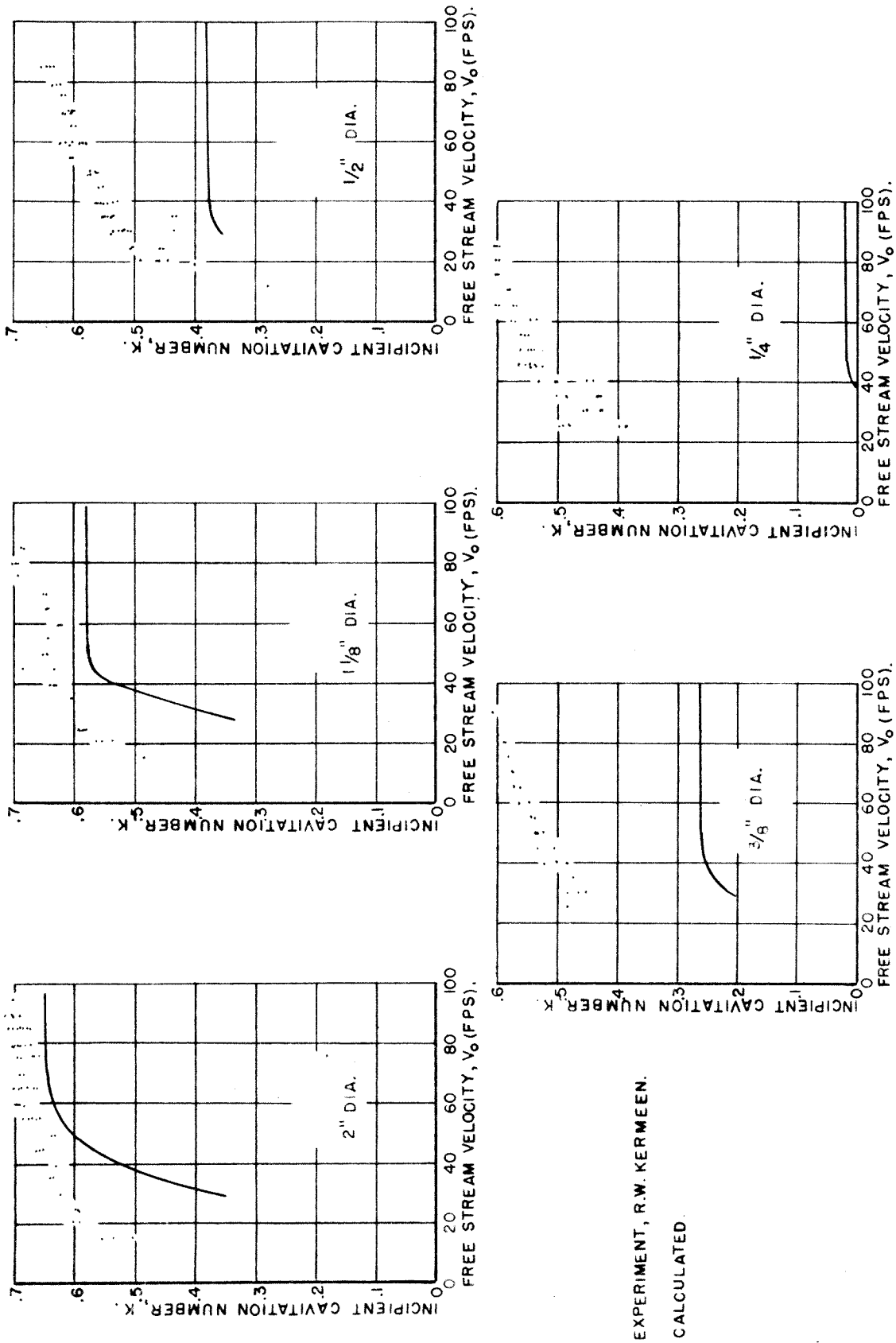

Fig. 29 - Calculated and experimental results for incipient cavitation on the "Hemispheres"

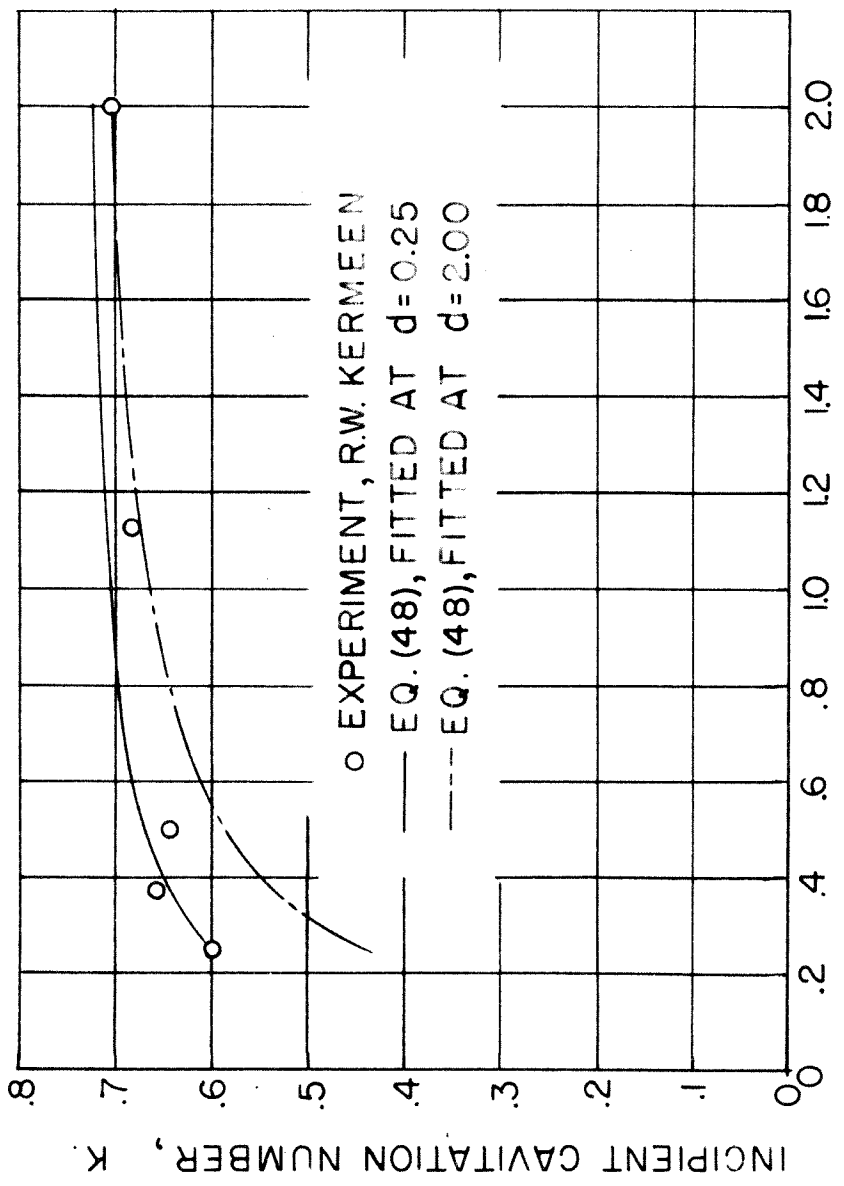

Fig. 30 - Experimental and calculated results for the inception of cavitation at high free stream velocity

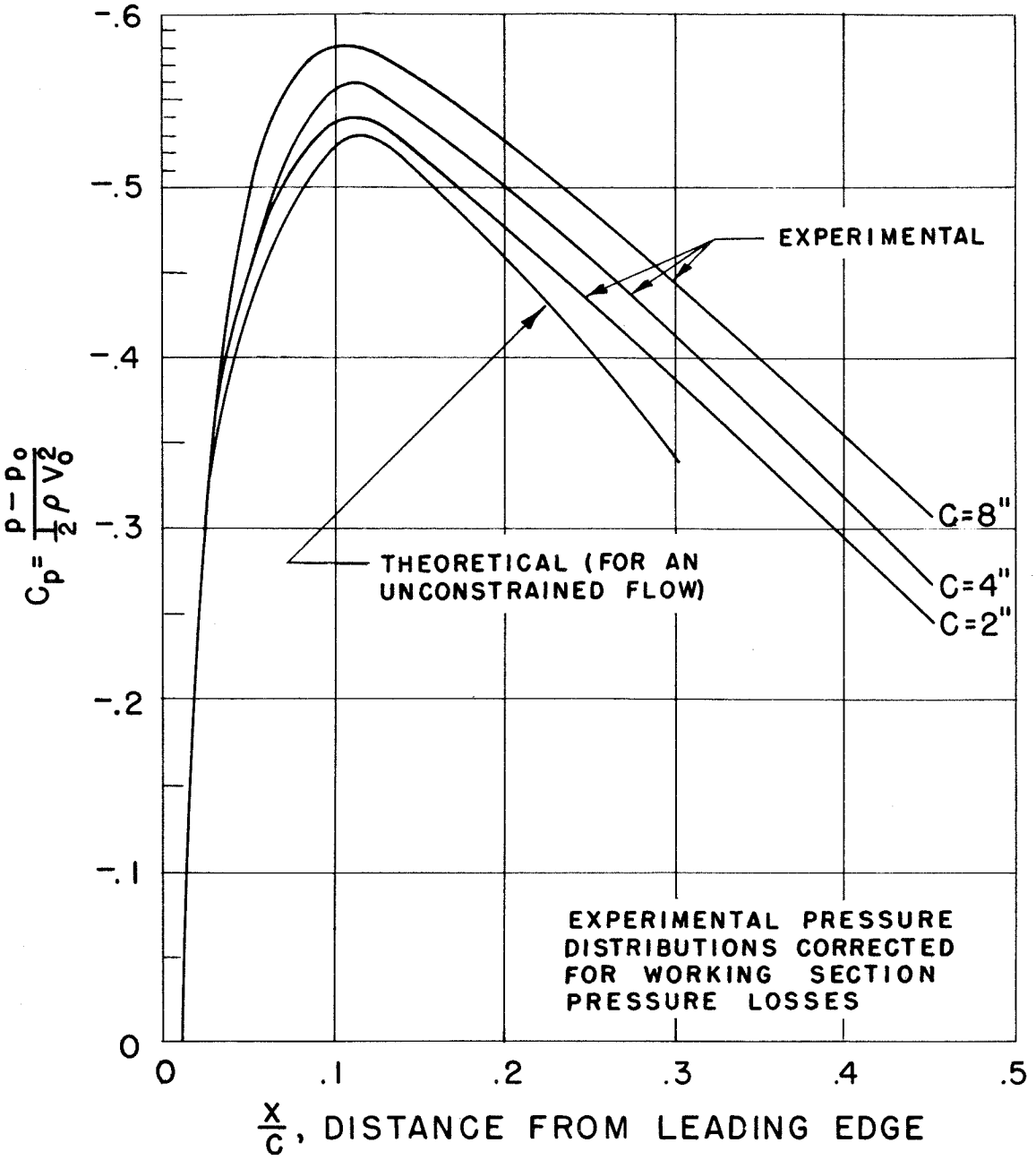

Fig. 31 - Faired pressure distributions over the Joukowski hydrofoils

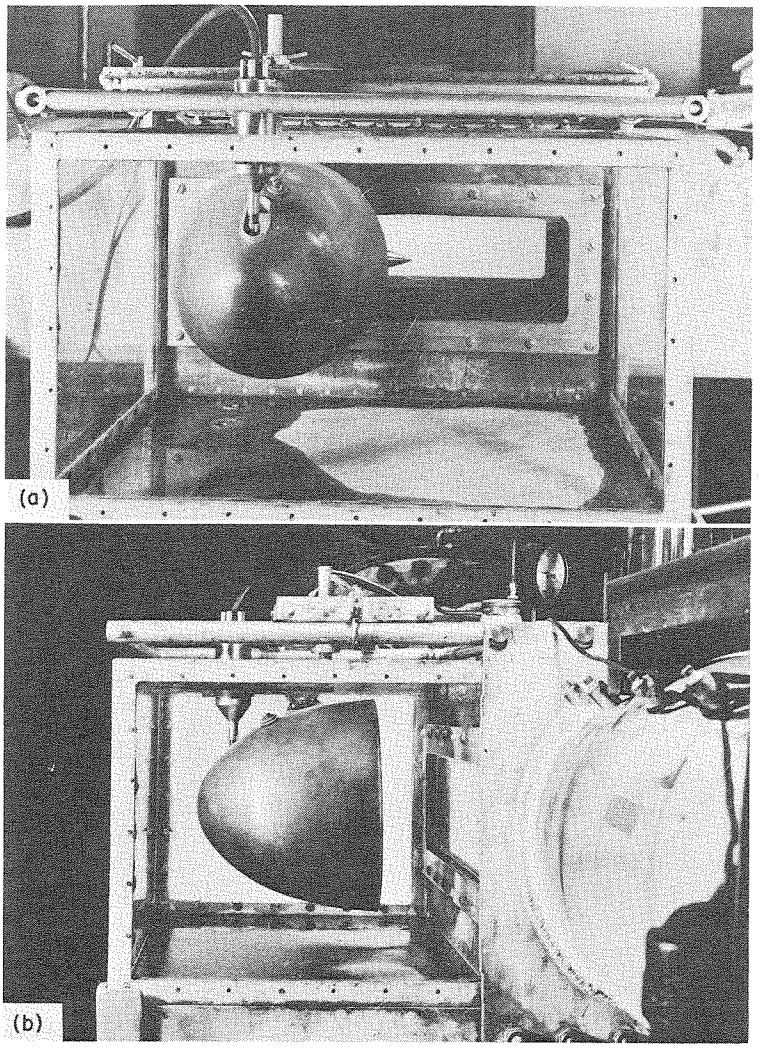

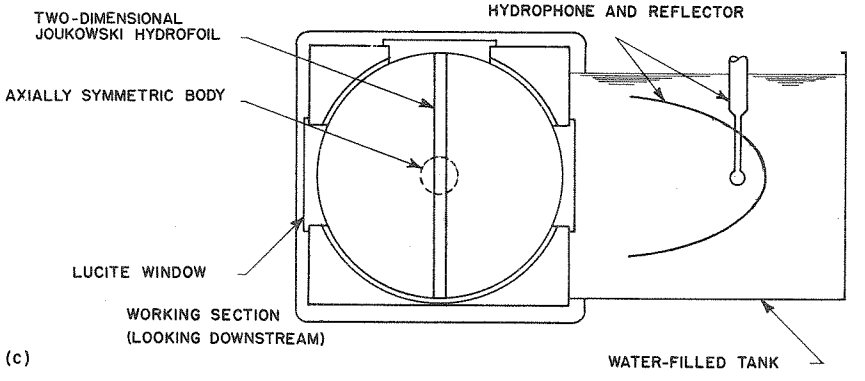

Fig. 32 - Arrangement of the sound measuring equipment

(a) Side view of the sound measuring apparatus installed on the water tunnel working section.

(b) View of the sound measuring equipment looking in the upstream direction.

(c) Schematic diagram of the sound measuring equipment.